NMR and laser Raman scattering studies of fluids at high pressure

1992 J. Phys.: Condens. Matter 4 305

(http://iopscience.iop.org/0953-8984/4/2/002)

J. Phys.: Condens. Matter 3 (1991) 305–338. Printed in the UK

REVIEW ARTICLE

NMR and laser Raman scattering studies of fluids at high pressure

J Jonas and Y T Lee
Department of Chemistry, School of Chemical Sciences, University of Illinois, Urbana, IL 61801, USA

Received 23 June 1991

Abstract. Recent developments in high-pressure studies of fluids using nuclear magnetic resonance and laser Raman scattering techniques are discussed in this review. Two topics are covered in the part dealing with nuclear magnetic resonance studies. First, an overview of pressure effects on self-diffusion in simple polyatomic fluids, water and complex liquids is presented together with their theoretical interpretation. Second, the promising field of high-pressure, high-resolution NMR spectroscopy of fluids is introduced using several recent studies. Both properties related to single-particle scattering and phenomena resulting from multi-body interactions in fluids are discussed in the review of Raman studies. In particular, high-pressure studies of collision-induced scattering are critically examined. The need for the separation of the effects of density and temperature on the dynamic and static structure of fluids represents the common denominator throughout the review. Therefore, in order to improve our understanding of fluids, all experimental studies of them should use pressure as an experimental variable.

Contents

0953-8984/92/020305 + 34 $04.50

1. Introduction

Our understanding of the liquid state has lagged far behind our basic knowledge of the solid and gas states. While there exists an ideal crystal lattice model for solids and an ideal gas model for gases, no such simple ideal model is available for liquids. This lag is due to the inherent complexity of liquids: they have neither the rigid geometric structure of solids nor the complete randomness of gases. In recent years, there has been significant progress toward a better understanding of the liquid state based on both theoretical and experimental work. In particular, studies in which pressure has been used as an experimental variable have contributed in a major way to the recent advances in our knowledge of liquids [1].

There are several fundamental reasons for performing experiments on liquids at high pressure:

(i) It is important to realize that changing temperature at constant pressure affects molecular motions in two distinct ways: not only is the average kinetic energy of the molecule changed, but there is always an accompanying change in the average volume available for the motion of the molecule. Only by using both pressure and temperature as experimental variables can one separate the effects of density and temperature on molecular motions. Due to the close packing of molecules in a liquid, even a small change in density can produce a considerable change in the molecular dynamics of the system; therefore, in order to test rigorously a theoretical model of a liquid, or a model of a specific dynamic process in a liquid, one must perform isochoric, isothermal, and isobaric experiments.

(ii) Use of pressure allows one to extend the range of measurements above the boiling point and also permits the study of supercritical dense fluids [2].

(iii) In an analogy to the concept of pressure tuning of energy levels in solids [3] one can pressure tune the intermolecular interactions in liquids [4].

(iv) Studies of re-orientational motions and reaction dynamics require variation of the solvent shear viscosity η. In most studies η is changed by the use of different solvents but in a high-pressure experiment η can be changed by changing pressure. Since introduction of different solvents changes the solute–solvent intermolecular potential the high-pressure single solvent experiment represents a much cleaner experiment [5].

As an illustration of the importance of separating the effects of density and temperature on molecular motions, figure 1 shows the temperature dependence of the self-diffusion coefficient, D, in liquid tetramethylsilane (TMS) at constant density and at constant pressure [6]. The dramatic difference in the temperature dependence of D at constant pressure and at constant density is readily apparent. Studies of intermolecular interactions and Fermi resonance provide examples of pressure tuning of intermolecular interactions in fluids. The Fermi resonance between the ν_1 and the first overtone of ν_4 has been studied in liquid ND_3 as a function of density and temperature [7]. Figure 2 shows the changes in relative intensities of these Fermi resonance coupled bands for the extreme density range of the measurements performed. Since Fermi resonance parameters are sensitive to intermolecular potential one can change them by varying temperature and pressure. The transition dipole moments of the $\nu_1 + 2\nu_4$ bands are found to vary as a function of density and the theoretical Fermi resonance treatment allows one to estimate the changes in their relative magnitude. In fact, the high-pressure experiments provide the critical spectroscopic information needed for the theoretical analysis of intermolecular interactions in ND_3.

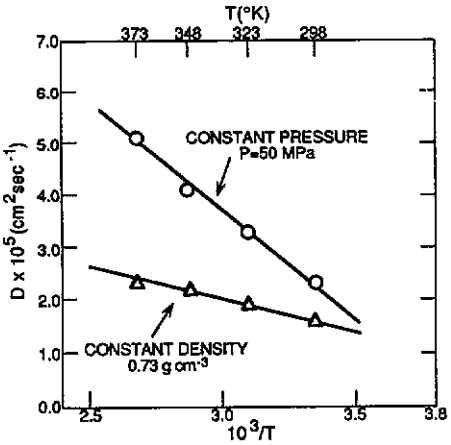

Figure 1. Temperature dependence of self-diffusion in liquid tetramethylsilane at constant pressure (○), and constant density (△). (Taken from [1].)

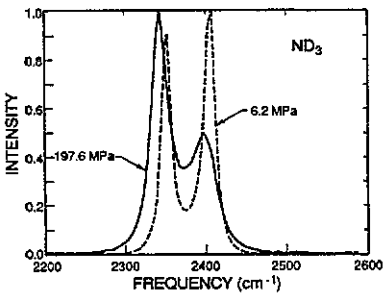

Figure 2. Density effects on the relative intensity of the isotropic $\nu_1 + 2\nu_4$ Fermi resonance lines in ND_3. The full curve denotes density $\rho = 0.73$ g cm^{-3} ($T = 0$ °C; $P = 197.6$ MPa), and the dashed curve denotes density $\rho = 0.457$ g cm^{-3} ($T = 100$ °C; $P = 6.2$ MPa). (Taken from [7].)

In view of our own research interests this article reviews recent high-pressure work on simple polyatomic molecular liquids using nuclear magnetic resonance, and laser Raman scattering techniques. This review is not intended to be comprehensive. Instead, discussion of the selected, specific results of high-pressure studies of the dynamical structure of liquids illustrates the type and scope of problems that can be investigated. In particular, our attention is focused mostly on work which has appeared since 1985. It is important to point out that maximum pressures of 1 GPa are usually used in studies of liquids which are relatively compressible; such pressures only change intermolecular distances. In contrast, for investigations of solids, pressures in excess of about 3 GPa are needed to affect the electronic molecular structure of the systems studied.

There are excellent recent reviews dealing with various aspects of high-pressure studies of fluids, e.g. the review of high-pressure NMR studies of water and aqueous solutions by Lang and Lüdemann [8] is of particular relevance to the topics discussed in the present article. Franck [9] reviews the field of supercritical dense fluids. Hensel [10] addresses the problem of critical behaviour of fluid metals, and Wakeham [11] reviews recent progress in the study of the thermal conductivity of liquids at high

pressure. Trends in high-pressure thermodynamics of fluid mixtures of non-electrolytes are surveyed by Schneider *et al* [12]. Recent advances of the theory of dense fluids with specific applications to the study of the shocked compressed liquids are discussed by Ross [13]. In his recent review article Baglin [14] discusses progress in laser Raman studies of fluids at high pressure.

2. NMR studies of fluids at high pressure

2.1. Information content of NMR experiments

NMR spectroscopy represents a well established and powerful tool for studying the dynamic structure of liquids. Since the application of various NMR techniques to investigate molecular motions and interactions in liquids has been discussed in detail elsewhere [15] only a few comments are given.

It is well known that an NMR signal from magnetic nuclei can provide detailed information about the nature and the rate of molecular motions. During the NMR relaxation experiment, after the spin magnetization is changed from its equilibrium value by a specific radio-frequency pulse, one determines the time constant of its return to equilibrium. This time constant, the spin–lattice relaxation time, T_1, is the time needed to reach thermal equilibrium between the spins and the lattice. The lattice is the collection of atoms of molecules that constitute the sample. Depending on the specific nucleus and the specific system, nuclei can relax by different mechanisms.

The dipolar, quadrupolar, and spin–rotation interaction mechanisms represent the main relaxation modes observed in studies of the dynamics of liquids. The relaxation process occurs through fluctuating magnetic and electric fields (for quadrupolar nuclei). Since these fluctuating fields have their origin in motions of the molecules in the liquid, the measured relaxation times provide information on molecular motions. Using well-known theoretical expressions, one can analyse the experimental spin–lattice relaxation times and determine the correlation times for the appropriate motion. One can determine the re-orientational correlation time, τ_θ, defined in the standard form

$$\tau_\theta = \int_0^\infty \langle P_2[\vec{u}(0) \cdot \vec{u}(t)]\rangle \mathrm{d}t / \langle P_2^2 \rangle \tag{1}$$

where P_2 is the second Legendre polynomial. When spin–rotation interactions dominate the relaxation mechanism the measurements of the NMR relaxation times yield the angular momentum correlation time, τ_J, defined as

$$\tau_J = \int_0^\infty \langle \vec{J}(0) \cdot \vec{J}(t)\rangle \mathrm{d}t / \langle J^2 \rangle \tag{2}$$

where J is the molecular angular momentum. The NMR spin–echo technique provides a convenient way to determine the self-diffusion coefficient, D, in a liquid or gas

$$D = \frac{kT}{m} \int_0^\infty \langle \vec{v}(0) \cdot \vec{v}(t)\rangle \mathrm{d}t / \langle v^2 \rangle \tag{3}$$

where v is linear velocity. Physically, a correlation time represents the average time the molecule needs to lose memory of its initial position, orientation, or angular momentum. The information content of the NMR relaxation experiments is very high. For example, by measuring the relaxation of nuclei at different parts of a molecule, one can learn how fast the molecule rotates about its different axes.

2.2. Self-diffusion

Since various NMR spin–echo techniques are well suited for the measurement of self-diffusion in fluids at high pressure [16] it is not surprising that [17] many NMR studies of diffusion have been reported. In order to provide some coverage of studies which have appeared before 1985 we include Table 1 in this review [18].

Modern perturbation theories of liquids have related both static and dynamic properties of a real fluid to those of corresponding purely repulsive systems. In the case of diffusion various modifications of the hard sphere model of liquids have been used in interpreting the experimental NMR self-diffusion data. This hard-sphere picture of liquids is based on the idea that ***when liquid density is high, approximately twice the liquid density***, the molecules are so closely packed that forces between molecules are due to harsh, short-ranged repulsive forces between nearest neighbours and the slowly varying attractive forces can be neglected.

2.2.1. Simple polyatomic molecular liquids. In the early studies of Jonas [19] of the self-diffusion in molecular liquids the rough hard sphere model as introduced by Chandler [20] was used to interpret the experimental data. According to Chandler the predicted self-diffusion coefficient for the rough-hard-sphere fluid is less than that for the smooth-hard-sphere fluid because of the coupling between the rotational and translational motions of the liquid. The self-diffusion coefficient D_{exp} of a real fluid can be approximated by a self-diffusion coefficient of the rough-hard-sphere fluid, D_{RHS}

$$D_{\mathrm{exp}} \approx D_{\mathrm{RHS}} = AD_{\mathrm{SHS}} \tag{4}$$

where D_{SHS} is the diffusion coefficient for the smooth-hard-sphere fluid and A is a parameter less than 1 whose magnitude reflects the effect of the translational rotational coupling. A volue for A of 1 would correspond to the perfectly smooth-hard sphere with no coupling between the translational and rotational motions. Chandler assumed that the parameter A is essentially constant, with negligible density and temperature dependence. The hard-sphere diffusion coefficient is given by the following expression

$$D_{\mathrm{SHS}} = \frac{\sigma(\pi RT/16M)^{1/2}C_{\mathrm{AW}}(\xi)}{Z_{\mathrm{CS}}(\xi) - 1} \tag{5}$$

where σ is the hard sphere diameter, M is the molecular weight, $C_{\mathrm{AW}}(\xi)$ is the correction factor, $Z_{\mathrm{CS}}(\xi)$ is the compressibility factor, and all other symbols have their usual meaning. The correction factor $C_{\mathrm{AW}}(\xi)$ as obtained by Alder *et al* [21] in their molecular dynamics calculations is

$$C_{\mathrm{AW}}(\xi) = \frac{D}{D_{\mathrm{E}}} \tag{6}$$

where D_{E} is the Enskog value for the self-diffusion coefficient. The Carnahan–Starling approximation for the compressibility factor is used

$$Z_{\mathrm{CS}} = \frac{1 + \xi + \xi^2 - \xi^3}{(1 - \xi)^3} \tag{7}$$

where the packing fraction is given as

$$\xi = \tfrac{1}{6}\pi\rho\sigma^3 \tag{8}$$

ρ being the number density and σ the hard-core diameter. In order to calculate the theoretical D_{RHS}, one can use the expression for D_{SHS} obtained by Dymond [22] by fitting the computer molecular dynamics results by Alder *et al* [21] in their study of the transport properties of the hard sphere fluid

$$D_{SHS} = 1735\left(\frac{T}{M}\right)^{1/2}\sigma\left(\frac{\sqrt{2}}{\rho\sigma^3} - 1.384\right) \tag{9}$$

where σ is the hard sphere diameter, M is the molecular weight, ρ is the number density, and other symbols have their usual meaning. The purpose of the studies of self-diffusion in liquids was to determine the hard sphere diameter from the density-dependence of the self-diffusion coefficients, D_{exp}, and then to compare the experimental D to those predicted theoretically. Selected results of studies of self-diffusion are summarized in table 1 which gives the hard sphere diameters for the liquids studied and the temperature coefficient $d\sigma/dT$. The hard sphere diameter is found to decrease with increasing temperature. Physically, this corresponds to the fact that the repulsive part of the potential has a finite slope. Assuming that at the turning point in a collision, the translational kinetic energy is converted to potential energy, then the molecules with high kinetic energy have higher potential energies corresponding to a smaller σ on the intermolecular potential curve.

Table 1. Self-diffusion in molecular liquids[a].

Liquid	Experimental range		σ (Å)	$(d\sigma/dT) \times 10^3$ (Å/K)	A[b]
	T (K)	P (MPa)			
$Si(CH_3)_4$	298–373	0.1–450	5.68(298)[c]	~ -0.7	0.56–0.62
SF_6	296–398	0.1–200	4.81(296)	−1.0	~ 0.97
C_4F_8	323–474	0.1–190	5.65(323)	−0.9	~ 0.9
$CFCl_3$	379–460	0.1–200	4.97(379)	−0.9	~0.6
$CClF_3$					
C_6H_6	303–433	0.1–450	5.12(303)	−0.6	0.77–0.82
C_6H_{12}	313–383	0.1–200	5.54(312)	−0.5	0.71–0.84
$C_6H_{11}CH_3$[d]	203–298	0.1–500	5.74(298)	−0.4	0.26–0.52
C_5H_5N[d]	303–423	0.1–500	4.94(303)	−0.34	$0.6 \sim 1.0$

[a] Original references given in review by Jonas [18].
[b] Hard sphere diameter σ.
[c] Range of A values for the temperature interval studied.
[d] The number in parenthesis gives the temperature in K.
[e] Modified RHS model; the parameter A is strongly temperature-dependent. The lower value of A corresponds to the lowest temperature of the temperature interval studied.

The parameter A is slightly temperature-dependent for liquids whose molecules are of nearly spherical shape but changes significantly in liquids composed of non-spherical molecules (see table 1). It is interesting to note that a modified RHS model which allows for a large change of A with temperature has been used to describe well the transport properties for pyridine [23]; there is independent spectroscopic evidence that there are specific interactions between pyridine molecules. In the case of molecules

of non-spherical shape such as methylcyclohexane [24], one has to allow for a large change of A with temperature (see table 1) to obtain agreement between experimental and predicted D.

In contrast to Chandler's approach who ascribed the difference between the predicted hard sphere diffusion coefficient D_{SHS} and the self-diffusion coefficient of real liquids to inelastic effects due to the coupling of rotational and translational motions, Speedy *et al* [25] proposed the so-called interacting sphere model based on Lennard–Jones potential which focused on the role of attractive forces in slowing down diffusive motions in polar fluids.

The experimental self-diffusion coefficient is expressed as

$$D_{\mathrm{exp}}(T, \rho\sigma_{\mathrm{B}}^3) = D_{\mathrm{LJ}} = D_{\mathrm{HS}}(T, \rho\sigma_{\mathrm{B}}^3, \sigma_{\mathrm{B}})A(T) \qquad (10)$$

where the symbols have their usual meaning. The hard sphere diameter σ_{B} is given by the equation

$$\sigma_{\mathrm{B}} = \sigma_{\mathrm{LJ}} \left(\frac{2}{1 + \left(2\frac{\epsilon}{kT}\right)^{1/2}} \right)^{1/6} \qquad (11)$$

where σ_{LJ} is the Lennard–Jones diameter, and ϵ is the well depth of the LJ potential. The parameter $A(T)$ in equation (10) is expressed as

$$A(T) = \exp\left(-\frac{\epsilon}{kT}\right). \qquad (12)$$

It is interesting to note that this approach represents very well the self-diffusion coefficients in various polar halomethane fluids as illustrated by table 2 taken from the original reference [25].

Table 2. Self-diffusion data for polar halomethane fluids interpreted by the interacting sphere model [25].

Substance	T(K)	$\rho\sigma^3$	σ_{LJ}(nm)	$(\epsilon/k_{\mathrm{B}})$(K)	% Std. dev.
CH_3Cl	210–440	0.53–0.88	0.436	129	8.2
CH_2Cl_2	186–406	0.65–1.02	0.479	162	3.3
$CHCl_3$	233–397	0.73–0.98	0.534	107	4.5
CH_3F	153–440	0.21–0.90	0.405	56	8.5
CHF_3	142–433	0.31–0.99	0.434	86	6.6
$CHClF_2$	147–383	0.49–1.04	0.461	164	6.8

In his recent study Lüdemann [26] has critically analysed the high-pressure self-diffusion data on a number of non-polar, polar, and hydrogen-bonded liquids including water. He pointed out that self-diffusion in fluids composed of spherical top molecules of tetrafluoromethane and methane can be described by using the simple expression for smooth hard sphere diffusion. In contrast, in polar fluids of methylfluoride and fluoromethane one has to use the full expression (equation (10)) for the interacting sphere model in order to interpret the diffusion data.

In addition Lüdemann concludes that even the interacting sphere model fails to describe quantitatively diffusion in alcohols which represent hydrogen-bonded fluids. However, various authors used the RHS model with variable rotational–translational coupling to interpret the experimental diffusion data in simple alcohol fluids [27] (see table 3).

Table 3. Self-diffusion in molecular liquids[a,b].

Liquid	Temp range (K)	Pressure range (MPa)	Theory[a,b]	Ref.
Methanol	278–328	0.1–300	RHS	[27]
Methanol-d_3	214–343	0.1–300	RHS	[27]
Ethanol	298	0.1–260	RHS	[27]
OMCTS[c]	323	0.1–58.4	RHS	[28]
N,N-dimethylformamide	288–313	0.1–280	RHS	[29]
N-methylformamide	288–313	0.1–280	RHS	[29]
Trifluoromethane	140–450	0.1–200	IHS	[30]
Tetrafluoromethane	140–432	0.1–200	IHS	[31]
Trichloromethane	217–397	0.1–150	RHS	[32]
	278–348	0.1–400		[33]
Dichloromethane	186–406	0.1–200	IHS	[32]
Chloromethane	186–440	0.1–200	IHS	[32]
Chlorodifluoromethane	145–400	0.1–200	IHS	[34]
Chlorotrifluoromethane	303,323,348	4–200	IHS	[35]
Bromotrifluoromethane	141–432	0.1–200	RHS	[31]
2-ethylhexyl benzoate	253–373	0.1–450	RHS	[36]
2-ethylhexyl cyclohexane carboxylate	253–353	0.1–450	RHS	[37]
Methylfluoride	150–450	0.1–200	RHS	[38]
Deutero-methylfluoride	150–450	0.1–200	RHS	[38]

[a] RHS: rough-hard-sphere model; IHS: interacting-hard-sphere model.
[b] IHS: interacting hard-sphere model.
[c] Octomethylcyclotetrasiloxane.

2.2.2. Water and aqueous solutions. Since Lang and Lüdemann [8] have recently reviewed in a comprehensive way the NMR studies of pressure effects on the dynamic behaviour of heavy water and aqueous solutions only a few brief comments are needed to highlight the anomalous behaviour of water when compared to other molecular liquids. In contrast to simple molecular liquids, the behaviour of water is quite complex and it is not surprising that the hard-sphere picture is not applicable to this important liquid. The most interesting behaviour of various transport and relaxation properties for water and heavy water occurs at temperatures between −15 and 40 °C. In normal fluids, compression and increased packing significantly slow down all motions; in water, on the other hand, the T_1, self-diffusion coefficients, and fluidity go through a maximum with initial compression, and only with further increases in pressure restrict motional freedom [15]. It is interesting to note that even the average residence time of a proton on a water molecule shows this anomalous behaviour with compression at temperatures below 40 °C [39].

The general effect of pressure and temperature on the dynamic properties of water is illustrated in figure 3, which shows the effect of pressure on self-diffusion in liquid heavy water in the temperature range −15 to 200 °C. Analogous plots can be drawn for any dynamic property of D_2O or H_2O. Another excellent example which compares the behaviour of water and supercooled water to that of simple fluorocarbon fluid has recently been provided by Lüdemann [26]. Specifically, the pressure dependence of translational and rotational mobility in water to that in methylfluoride fluid is depicted in figure 4 which compares the reduced isotherms for translational and rota-

tional mobility in H_2O and CH_3F fluid. Indeed, the anomalous motional behaviour of supercooled water (243 K isotherm) in contrast to hot water (363 K isotherm), and the 'normal' fluid of CH_3F is well illustrated in this figure.

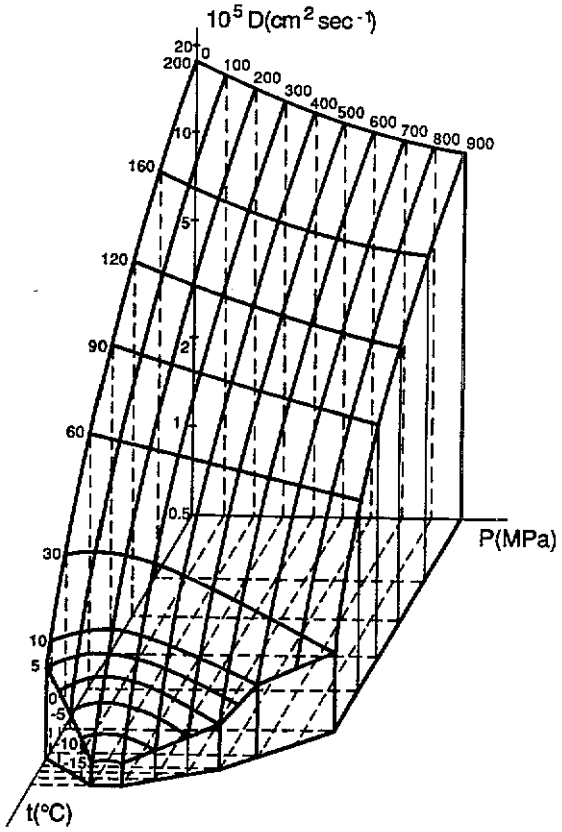

Figure 3. Self-diffusion as a function of temperature and pressure in liquid D_2O. (Taken from [15].)

The anomalous motional behaviour of water molecules with initial compression can be qualitatively interpreted in terms of a simple physical picture based on changes in the random hydrogen-bond network [15]. The characteristic structural feature of liquid water is the local tetrahedral environment of each molecule, beyond which there is a randomized imperfect space-filling network of hydrogen-bonded molecules. By compressing liquid water in the selected low-temperature range, we affect the hydrogen-bond network and gradually go from optimal tetrahedral order toward a more compact packing arrangement. There is a competition in water between the tendency of strongly directional forces to build an open, hydrogen-bond network and the tendency for external pressure to pack the molecules together more efficiently. Since the process for self-diffusion, shear viscosity, and re-orientation of the water molecules necessitates the breaking and reforming of hydrogen bonds, one can expect that it will be easier to break an already bent hydrogen bond than an undistorted one. Initial compression, therefore, increases motional freedom, and only further compression slows down all the hydrodynamic processes because of a more compact packing of the water molecules.

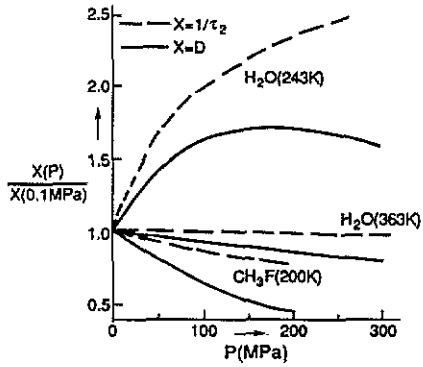

Figure 4. Reduced isotherms of the pressure dependence of the inverse rotational correlation times $1/\tau_2$ and the self-diffusion coefficients D in H_2O and CH_3F liquids. (Taken from [26].)

Under high compression the repulsive hard core interactions begin to compete strongly with the directional forces that are responsible for the open structure of water at low pressures and low temperatures.

2.2.3. Applicability of hydrodynamic Stokes–Einstein equation at the molecular level. The results of a ^{1}H NMR studies [36,37] of self-diffusion in complex liquids of 2-ethylhexylbenzoate (EHB) and 2-ethylhexylcyclohexanecarboxylate (EHC) over a wide range of temperatures (−20 to 100 °C) and pressures (0.1 to 450 MPa) were of intrinsic interest as the study utilized two different NMR methods [16] to obtain self-diffusion data over the wide range of fluid viscosities accessible (1 to approximately 90 000 cP). The resultant diffusion coefficients (D) of the system ranged from around 10^{-5} to 10^{-10} cm^2 s^{-1}, which represents an unprecedented range to be directly measured for a single fluid system. Interest in this fluid was prompted by a lack of understanding of the relationship between the molecular properties and bulk fluid properties of elastohydrodynamic (EHD) lubricants, which operate under conditions of high pressure. In this respect EHB has been chosen as a model synthetic hydrocarbon based EHD lubricant, its molecular structure being complex enough to represent a real EHD fluid, while still being simple enough to allow spectroscopic probing of its molecular dynamics. Indeed, the wide range of fluid viscosities readily accessible using the pressure and temperature capabilities in our laboratory is indicative of the fluid's suitability as a model lubricant.

The availability of a wide range of diffusion coefficients and viscosities enabled us to provide a test of the Stokes–Einstein equation at the molecular level for EHB and EHC. This hydrodynamic equation relates the diffusion coefficient (D) to viscosity (η) and molecular radius (a) according to

$$D = \frac{kT}{C\pi a\eta} \tag{13}$$

where C is a constant equal to 4 in the slipping boundary limit and 6 in the sticking boundary limit. Equation (13) is derived for a macroscopic sphere moving in a continuum, and thus theoretically should only apply to solute–solvent systems where the solute is large compared with the solvent; in this case the stick condition ($C = 6$) should

apply. It has been suggested [40] that the slip condition ($C = 4$) may be approached when the solute and solvent are of similar size (i.e. self-diffusion). Interestingly, several studies have shown that equation (13) proves a reasonable estimate of self-diffusion for a number of simple molecules such as cyclohexane [41], methylcyclohexane [24], and benzene [42]. Figure 5 compares the experimental pressure dependence of the self-diffusion coefficient for liquid EHB and EHC with the theoretical predictions from viscosity using (13) in the slipping and sticking boundary conditions.

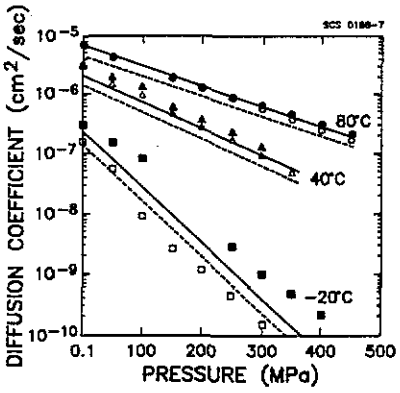

Figure 5. Self-diffusion coefficient of liquid EHB (open symbols) and EHC (full symbols) as a function of pressure in the temperature range −20 °C to +80 °C. The lines represent the predictions from the experimental shear viscosity using the Stokes–Einstein equations in the slip boundary limit (full curve) and the stick boundary limit (broken curve). (Taken from [46].)

All values of C at 80 °C approach the slipping boundary limit of 4, as would be expected in the case of self-diffusion. At 40 °C, the values of C for 2-EMC typically fall short of the slip limit to about $C \simeq 3$. It is interesting to consider, though, the microfriction correction to the Stokes–Einstein equation as proposed by Gierer and Wirtz [43] leads to $C = 3.4$. It is interesting to note that low values of C have also been observed for methylcyclohexane [24] and pyridine [23].

In view of the non-spherical shape and conformational flexibility of 2-EHB and 2-EHC liquids, it is quite impressive to find that the Stokes–Einstein equation can describe reasonably well the diffusive behaviour over such a wide range of viscosities and diffusivities. The validity of the Stokes–Einstein equation for highly viscous liquids offers an interesting opportunity for the workers in the applied field of lubrication. Since the experimental techniques used to measure shear viscosities of highly viscous liquids at high pressure are relatively cumbersome and inaccurate, the Stokes–Einstein equation provides a good estimate of the shear viscosity when the diffusion data are available. In view of the fact that the various NMR spin–echo and rotating-frame relaxation techniques for the measurement of self-diffusion coefficient are well suited for work at extreme conditions of high pressure and temperature, the NMR approach may find its use in the lubrication field as a convenient way for the determination of shear viscosities of lubricants at extreme conditions.

2.3. High resolution NMR experiments

The large majority of NMR applications in chemistry deal with liquids in which the NMR lines are narrowed by motional averaging to a natural line width of the order of

0.1 to 1 Hertz. High-resolution NMR spectra of complex molecules in the liquid phase usually exhibit a great deal of structure and yield a wealth of information about the molecule. Therefore, it is not surprising that the multi-nuclear high-resolution Fourier transform NMR spectroscopy at high pressure represents the most promising technique in the studies of the dynamics in liquids [44]. The high information content of the many advanced NMR techniques including 2D-NMR techniques such as NOESY, COSY, and ROESY have yet to be fully explored in the high-pressure NMR experiments. Recent advances in superconducting magnet technology have resulted in the development of superconducting magnets capable of attaining a high homogeneity of the magnetic field over the sample volume so that even without sample spinning one can achieve high resolution. It is quite impressive that one is able to achieve a NMR line width of 1 Hz for sample diameter of 8 mm at the proton frequency of 300 MHz ($H_0 = 7.0$ tesla). At the same time, Fourier transform techniques make all these high resolution experiments much easier to be performed at high pressure than was the case with classical CW techniques.

There are several recent reviews dealing with chemical applications of high resolution, high-pressure NMR; e.g. studies of kinetics of solvent exchange reactions at high pressure [45], applications to biochemical systems [46], and applications of NMR capillary techniques to a variety of chemical problems in liquid solutions [47].

2.3.1. Natural abundance ^{13}C relaxation in complex liquids. Both experimental and theoretical studies have demonstrated the value of natural abundance ^{13}C NMR relaxation experiments to yield a detailed information about the motional dynamics of complex liquids. So far, however, all such ^{13}C NMR studies have been performed only as a function of temperature at atmospheric pressure. Taking advantage of our recent development [48] of NMR instrumentation which permits high resolution, high sensitivity NMR experiments on liquids at high pressure, we decided to measure natural abundance ^{13}C NMR spin–lattice relaxation times, T_1, and Nuclear Overhauser Enhancement (NOE) in liquid 2-ethylhexyl cyclohexanecarboxylate (EHC) and 2-ethylhexyl benzoate (EHB) as a function of pressure from 0.1 MPa to 500 MPa within the temperature range from −20 °C to +80 °C [49]. The general expressions relating ^{13}C T_1 and NOE to the spectral density functions for the intramolecular dipolar coupling mechanism are

$$\frac{1}{NT_1} = \frac{\hbar^2\gamma_c^2\gamma_H^2}{10r_{cH}^6}\left[J(\omega_H - \omega_c) + 3J(\omega_c) + 6J(\omega_H + \omega_c)\right] \tag{14}$$

$$\text{NOE} = 1 + \frac{\gamma_H}{\gamma_c}\left(\frac{6J(\omega_H + \omega_c) - J(\omega_H - \omega_c)}{J(\omega_H - \omega_c) + 3J(\omega_c) + 6J(\omega_H + \omega_c)}\right) \tag{15}$$

where N is the number of directly attached protons, $J(\omega)$ is the spectral density function, and ω_H and ω_c are the proton and carbon resonant frequencies, respectively. The particular form of $J(\omega)$ depends on the model for molecular re-orientation. Because of asymmetric shape and high degree of internal mobility in EHC and EHB, the form of $J(\omega)$ needed to describe the relaxation is complex.

Figure 6, which gives the natural abundance ^{13}C NMR spectra of liquid EHB obtained at 80 and 500 MPa pressure, illustrates the excellent resolution obtainable even under high-pressure conditions without sample spinning. This high resolution permits the ^{13}C T_1 measurements for each individual carbon in EHC and EHB (total of 15 carbon atoms in the molecule) and makes it possible to probe directly the overall and

internal motions in these complex liquids. The fact that our experiments covered both the motionally narrowed regime and the slow-motion regime as viscosity changes extend over five orders of magnitude enabled us to test rigorously the various theoretical models proposed to describe the dynamics of complex molecules of asymmetric shape and high flexibility.

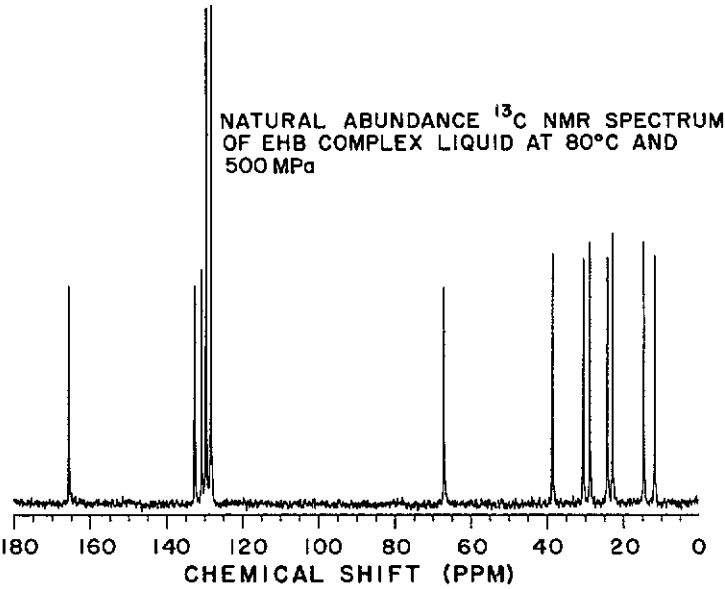

Figure 6. High resolution, natural abundance ^{13}C NMR spectrum of EHB at 80 °C and 500 MPa. (Taken from [49].)

A detailed analysis of the ^{13}C T_1 and NOE data is given in the original reference [49] and at this point we mention a few selected results. In order to interpret the relaxation data it was necessary to write the spectral density in terms of distribution of isotropic re-orientational times defined by

$$J(\omega) = \int_0^\infty \frac{G(\tau)\,\tau\,\mathrm{d}\tau}{1+\omega^2\tau^2} \tag{16}$$

where $G(\tau)$ is a probability density function such that

$$\int_0^\infty G(\tau)\,\mathrm{d}\tau = 1\,. \tag{17}$$

The Cole–Davidson distribution, with a characteristic limiting correlation time τ_0, has successfully described pressure effects on re-orientation in glycerol [50]. The probability density function takes the form

$$G(\tau) = \begin{cases} \dfrac{\sin(\beta\pi)}{\pi}\left(\dfrac{\pi}{\tau_0-\tau}\right)\beta & \text{for } 0 \leqslant \tau < \tau_0 \\ 0 & \text{for } \tau \geqslant \tau_0\,. \end{cases} \tag{18}$$

In equation (18), β is the distribution width and may assume a value from 0 to 1. When $\beta = 1$, this implies that one correlation time is present and the resulting spectral density function is equal to that of the isotropic model. As β approaches 0, the distribution becomes wider until infinitely many correlation times are assumed in the $\beta = 0$ limit. The representative fits of EHB and EHC NT_1's plotted against pressure using the Cole–Davidson distribution model are shown in Figures 7 and 8. The model clearly represents the experimental data well.

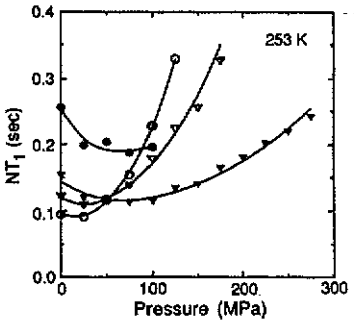

Figure 7. Pressure dependence of EMB and EHC ^{13}C NT_1 at 253 K fitted by using the Cole–Davidson distribution model: (○) EHB carbon 5; (▽) EHB carbon 9; (●) EHC carbon 5; (▼) EHC carbon 9. (Taken from [49].)

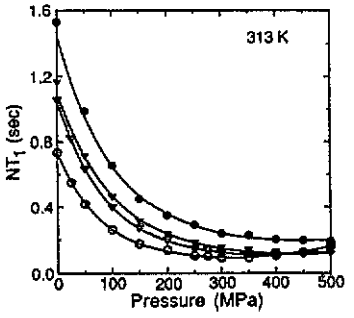

Figure 8. Pressure dependence of EMB and EHC ^{13}C NT_1 at 313 K fitted by using the Cole-Davidson distribution model: (○) EHB carbon 5; (▽) EHB carbon 9; (●) EHC carbon 5; (▼) EHC carbon 9. (Taken from [49].)

In conclusion, the results of this study illustrated the promising future of high-pressure, high-resolution NMR techniques to yield unique data of high information content on motional dynamics of complex liquids. A wide spectrum of both basic and technological fields ranging from dynamics of biopolymers to lubrication will benefit from the improved understanding of the dynamical behaviour of complex liquids.

2.3.2. Chemical shift studies. It is somewhat surprising that the number of high resolution NMR studies dealing with pressure effects on chemical shifts in liquids is quite limited [51–53]. It is not surprising to find that the study of pressure and temperature dependence of the proton chemical shift in water showed an anomalous pressure

behaviour of the chemical shift in the temperature range 5 °C to approximately 40 °C [53].

The studies of pressure effects on proton chemical shifts in simple alcohols left many questions unanswered. A recent study of liquid methanol by Schulman *et al* [54] illustrated well the possible problems when interpreting the experimental results obtained in high-pressure NMR studies of simple alcohols. Their analysis suggested just the opposite changes in hydrogen bonds with pressure than the earlier interpretation of diffusion data in methanol [55]. For example, it is well known that both increased temperature and dilution by inert solvents produces an upfield shift of the hydroxyl proton, reflecting an increased shielding of the proton. The prevalent interpretations of these changes are based on changes in the average degree of association favouring a large fraction of disrupted or distorted hydrogen bonds at higher temperature, and/or higher dilution with inert solvent. In the high-pressure NMR study of ethanol [52] the increasing density produced just the opposite effect on the hydroxyl proton chemical shift to that observed for the temperature increase. This would be compatible with the view that increasing density at all temperatures favours formation of a more extensive hydrogen bond network in ethanol or other alcohols. Further experiments on the effects of density and temperature on hydrogen bonds in various alcohols are needed in order to advance our understanding of hydrogen bonded fluids.

3. Raman scattering studies of fluids at high pressure

3.1. Information content of Raman experiments

As mentioned in section 2.1 the NMR relaxation experiment enables one to obtain the correlation time for a specific motion. One has to realize that a correlation time is the integral of the appropriate correlation function, therefore the great advantage of Raman experiments lies in the fact that the analysis of the Raman lineshape provides information about the detailed nature of the correlation function—one obtains the time dependence of the correlation function itself and not only an integral. However, the Raman experiment has some limitations, namely, only Raman lineshapes of relatively simple molecules can be analysed to yield unambiguous results. As the general theory of light scattering is well established a few comments about the Raman experiments are appropriate at this point.

From the experimental polarized and depolarized Raman bandshapes one can obtain the isotropic scattering intensity $I_{\mathrm{iso}}(\nu)$ and the anisotropic scattering intensity $I_{\mathrm{aniso}}(\nu)$. Only vibrational (non-orientational) processes contribute to $I_{\mathrm{iso}}(\nu)$ whereas both re-orientational and vibrational processes contribute to $I_{\mathrm{aniso}}(\nu)$. This provides the means of separating re-orientational processes from vibrational processes. The overwhelming majority of Raman studies of the dynamic processes in liquids dealt with the investigation of the properties of individual molecules by studying the re-orientational and vibrational relaxations which reflect only indirectly the influence of intermolecular interactions. Therefore, the problem of collision-induced scattering (CIS) has recently attracted both theoretical and experimental interest [56]. It has been observed that collisions in dense liquids or gases produce depolarized Rayleigh spectra in fluids composed of atoms or molecules of spherical symmetry. Collision-induced Raman spectra, forbidden by selection rules (symmetry), have been investigated in polyatomic molecular liquids as well as collision-induced contributions to the allowed

Raman bands. The origin of these collision-induced spectra lies in the polarizability changes produced by intermolecular interactions. It is clear that studies of CIS can provide direct information about intermolecular interactions. However, the CIS represents a very difficult theoretical problem because the scattered intensity depends on the polarizability change in a cluster of interacting molecules, and the time dependence of this change is a function of the intermolecular potential.

3.2. Pressure effects on frequency shifts

The vibrational frequency shifts of a free gaseous molecule, such as O_2, are in general different from those of liquid oxygen. The first attempt to explain the changes in the peak frequency is due to Benson and Drickamer [57] who pointed out that the difference ($\Delta\nu$) between the observed shift (ν) and the free-molecular value (ν_0) reflects the anharmonicity of the intramolecular potential perturbed by the interactions with neighbouring molecules. Therefore, the measurements of vibrational frequency shifts $\Delta\nu = \nu - \nu_0$ offer a means to study the molecular dynamics of fluids. For stretching vibrations, the increased attractive interactions result in a red shift ($\Delta\nu < 0$) whereas the enhanced repulsive interactions cause a blue shift ($\Delta\nu > 0$). Whether $\Delta\nu$ is larger than zero or smaller than zero is determined by the interplay of attractive and repulsive forces exerted on the observed molecule by the surrounding medium. This simple model has been successfully tested in a number of high-pressure studies as the changes in frequency shift can be written as

$$\Delta\nu = \Delta\nu_R + \Delta\nu_A \tag{19}$$

where, $\Delta\nu_R$, and, $\Delta\nu_A$, are the frequency shift due to the repulsive forces and attractive force, respectively.

Schweizer and Chandler [58] derived theoretically the explicit form for the frequency shift due to the repulsive forces, $\Delta\nu_R$

$$\Delta\nu_R = -\left(\frac{3K}{\mu^2\nu_0^3} + \frac{1}{4\mu\nu_0 L}\right)\langle F_R\rangle \tag{20}$$

where K is anharmonic force constant, L is the range of the repulsive forces, and μ is the reduced mass of the oscillator. The repulsive force F_R is determined from the slope of the two-point cavity distribution function, y_{HS}

$$F_R = -kT\left(\frac{\mathrm{d}\ln y_{HS}}{\mathrm{d}r}\right) \tag{21}$$

where

$$\ln y_{HS}(r) = \sum_{n=0}^{3} \frac{a_n(r-\sigma)^n}{\sigma^n} \tag{22}$$

and r is the bond length of two hard-sphere cavities of diameter σ. The coefficients a_n, which have been calculated by Pratt *et al* [59], are functions of the solvent's reduced density $\rho_r = \rho_s\sigma_s^3$ and the solute to solvent diameter ratio, σ/σ_s. The shift due to the attractive forces, $\Delta\nu_A$, can then be calculated by subtracting $\Delta\nu_R$ from the experimentally observed shift, $\Delta\nu$.

In the high-pressure study of liquid methanol [60], the Schweizer–Chandler (SC) model was used to evaluate the frequency shift of the ν_3-mode, C–H vibration, at various densities. It was found that the intermolecular interactions, as probed by the C–H vibrations, are dominated by the repulsive forces. The same conclusion was also obtained from the line shape analysis based on the SC model. However, the SC model is derived for simple, non-associated liquids, and hence, may not be applicable for modes strongly affected by the hydrogen bonding, such as the C–O vibration in liquid methanol.

Based on the SC model and empirical observations, Zakin and Herschbach [61] proposed a more simple formula for $\Delta\nu_R$ as function of the reduced density, ρ_R

$$\frac{\Delta\nu_R}{\nu_0} = c_1 \exp(m_1\rho_r) + c_2 \exp(m_2\rho_r) - c_3 \exp(m_3\rho_r) \tag{23}$$

where the coefficient c_n and m_n are defined in the original paper and can be determined from the molecular properties of the solute and solvent pair studied. Applying this formula to the ring breathing vibrations of neat liquid pyridine, benzene, toluene, and to solutions of pyridine in several solvents, they found that the pressure derivative, $d\nu/dp$, is dominated by the hard-sphere repulsion in the associated solvents. While the attractive part of the frequency shift, $\Delta\nu_A$ is generally negative, it can be positive in the aqueous pyridine solutions. Furthermore, $\Delta\nu_A$ varies only slightly with pressure and is not necessarily proportional to the solvent density as it was assumed in the SC model. For illustration we include figure 9 taken from work by Zakin and Herschbach. This figure shows the density dependence of the frequency shifts for representative C–H and O–H stretching modes for n-butylchloroform and n-butylalcohol in carbon disulfide solutions.

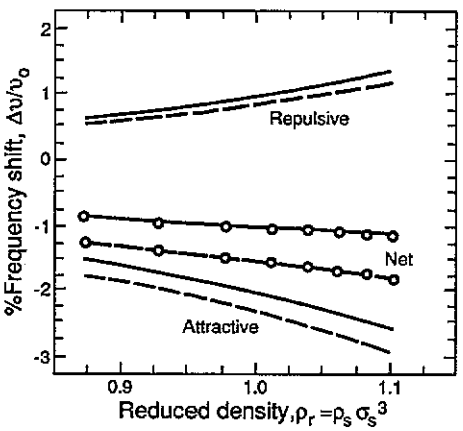

Figure 9. Frequency shifts for typical C–H and O–H stretching modes in solution ($CHCl_3$ and n-BuOH, respectively, in CS_2), as a function of reduced density. Solid curves for C–H of $CHCl_3$; dashed curves for O–H of n-BuOH. The repulsive contribution calculated from the hard sphere model, whereas the attractive contribution obtained by deducting the repulsive contribution. (Taken from [62].)

In fact, Zakin and Herschbach [62] found that for quasidiatomic C–H or O–H stretching vibrations

$$\frac{\Delta\nu_A}{\nu_0} = A\rho_r^{S_A} \tag{24}$$

with exponents $S_A = 2.1 \pm 0.3$. This expression was found valid for ten different fluid systems. The empirical S_A value can also be obtained theoretically by assuming an

attractive potential, R^{-n}. It was shown that the assumption in the SC model, (i.e. $S_A = 1$) is valid only in the zero-density limit and, in addition, the attractive frequency shift at high density depends more on the packing effects rather than on any specific form of intermolecular interactions. For R^{-n} attractive potential, an explicit formula for the $\Delta\nu_A$ was derived

$$\frac{\Delta\nu_A}{\nu_0} = c_4 \exp(m_4\rho_r) + c_5 \exp(m_5\rho_r) \tag{25}$$

where c_4, c_5, m_4 and m_5 can be calculated from the molecular properties and the known attractive potential.

3.3. Reorientational motions in fluids

During the past two decades re-orientational motions of molecular liquids and gases have been extensively studied by Raman lineshape analysis. High-pressure laser Raman scattering experiments provided conclusive evidence for the need to separate the effects of density and temperature on re-orientational processes in liquids. In order to illustrate the large difference between isobaric and isochoric experiments, figure 10 shows the rotational correlation functions for liquid methyl iodide (CH_3I), a symmetric top molecule. The correlation function describes the re-orientation of the CH_3I about axes perpendicular to the main symmetry axis.

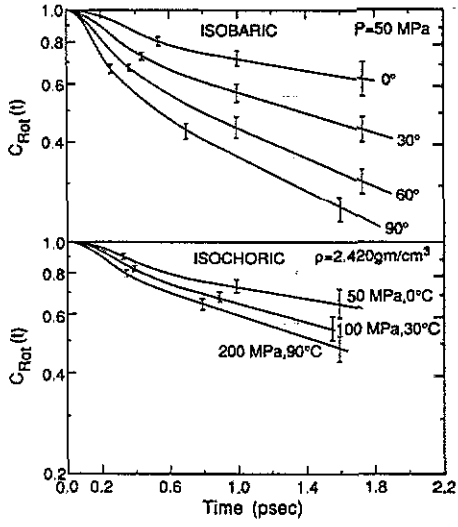

Figure 10. Temperature dependence of the rotational correlation function for liquid methyl iodide (CH_3I) under isobaric and isochoric conditions. (Taken from [1].)

At this point, it is worthwhile to point out the specific results of several such studies, which showed that the rotational second moment is strongly pressure/density dependent. According to classical interpretation, the second moment $M_R(2)$ is related to the rotational kinetic energy of the molecule and should not change with density. Its value is constant at a given temperature, $M_R(2) = 6kT/I_\perp$. ($I_\perp$ is the molecular moment of inertia perpendicular to the symmetry axis.) In contrast to this classical prediction we found that $M_R(2)$ is strongly density dependent in liquid chloroform

[63] and propyne [64]. In these cases we found that $M_R(2)$ decreases with increasing density.

For example, for the $\nu_1(A_1)$ C–H stretching mode in liquid chloroform [63] at 303 K there is a decrease of $M_R(2)$ from 510 cm^{-2} to 223 cm^{-2} with a density increase from 1.47 to 1.78 g cm^{-3}. The decrease of the second-moment with increasing density can be explained in terms of collision induced scattering (CIS) which contributes to the wings of the Raman band. The fact that the CIS affects only the far wings of the band explains why this effect was very often neglected; the correlation functions and the correlation times are affected only slightly. However, second-moment analysis, which describes the short time behaviour of a correlation function and thus reflects the collision-induced high-frequency contributions to the spectral line rather strongly, is the most reliable method of investigating short-time intermolecular interactions. The reason why the second moment decreases with increasing density is related to the decrease of collision-induced scattering with increasing density. Clearly, dynamic effects are not as inefficient, over short time intervals, as had been previously assumed. Evidently, three- and four-particle correlations must be included in any description of the scattering process. In their molecular dynamics calculations Alder *et al* [65,66] investigated the effects of density on bandshapes of depolarized light scattering from atomic fluids, taking into account not only two-particle but also three- and four-particle correlations. At low densities the pairwise term dominates and increases with density whereas at higher densities cancellations occur between the pairwise, triplet and quadruplet terms with the result that the total scattering intensity decreases. We proposed [63,64] that an analogous process is responsible for the decrease of CIS with increasing density in our liquid studies. The observed density dependence of the rotational second moment makes questionable studies using Raman bandshapes to calculate torques in liquids.

In this context, it is interesting to note that, in their study of ethane in the temperature range from 50 °C to 125 °C and pressure ranging from 0.1 bar to 200 MPa, Baglin et al [67] found that rotational second moment calculated from the ν_3 band is pressure and temperature independent. In view of this result it is important that additional high-pressure experiments address this problem.

3.4. Vibrational dephasing in fluids

Many different theories dealing with dephasing have been developed (for review, see [68]), examples of which are the isolated binary collision (IBC) model [69,70], the hydrodynamic model [71], the cell model [72], and the model based on resonant energy transfer [73].

In the measurements of isotropic line shapes of the C–H, C–D, and C–C stretching modes in a variety of simple molecular liquids [63], it was found that the IBC model [69,70], which considers only the repulsive part of the intermolecular potential in calculating the dephasing rate, reproduces the general trends of the experimental data observed. It should be pointed out that this model and other models predict that the dephasing rate (line width) will increase with density at constant temperature; therefore, it was interesting to observe a very different behaviour of the dephasing rate in liquid isobutylene ($CH_2 = C(CH_3)_2$) [74].

In order to understand this behaviour, one has to realize the different character of these two vibrations of interest. First, the $C{=}CH_2$ vibration is strongly infrared active, while the $C{-}CH_3$ vibration is inactive. Secondly, the classical vibrational amplitudes show that the repulsive forces of the bath may affect the $C{-}CH_3$ vibration more.

The Raman line shapes of the $\nu_4(A_1)$ symmetry C=CH_2 stretching mode of 1657 cm^{-1} and the $\nu_9(A_1)$ symmetric C–CH_3 stretching mode of 807 cm^{-1} in isobutylene [74] were measured as a function of pressure from vapor pressure to 0.8 g cm^{-3}, over the temperature range from −25 to 75 °C. Figure 11 shows the density dependence of the experimental half width $\Gamma = (2\pi c\tau_v)^{-1}$, where τ_v is the dephasing time and Γ is proportional to the dephasing rate. From figure 11 we see that increasing density, at constant temperature, affects the bandwidths of the two vibrations in a qualitatively different way. The C–CH_3 stretching bandwidth increases with increasing density, a behaviour found for many other models of liquids. This basic trend can be predicted in terms of an IBC model based on rapidly varying repulsive interactions. The most interesting result of this study was the observed decrease of the bandwidth of the C=CH_2 stretching mode (strongly infrared active band) with increasing density. To our best knowledge, this was the first experimental observation of a decrease in dephasing rate with increasing density in a liquid. It appears that this band is inhomogeneously broadened as it is affected by environmentally induced frequency fluctuations. These fluctuations are due to dispersion, induction, and electrostatic forces that depend on the dipole and polarizability of the molecule. The decay of the inhomogeneous environment around a molecular results in motional narrowing. The correlation function modelling [75], which uses the Kubo stochastic lineshape theory [76], was in agreement with the experimental data. In further studies we found a similar decrease in bandwidth for the C=O stretching mode in liquid acetone [77]. Again, the attractive interactions influence the dephasing process and are responsible for the density behaviour of the bandwidth.

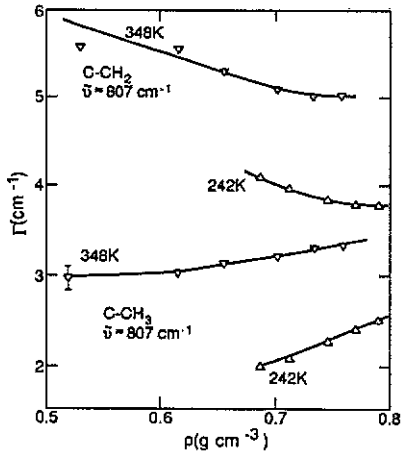

Figure 11. The density dependence of the experimental half-widths Γ for the C–CH_3 and C=CH_2 stretching modes in liquid isobutylene at 242 K and 348 K. (Taken from [74]a.)

The Raman experiments on isobutylene and acetone have been discussed in a theoretical study of dephasing by Schweizer and Chandler [58], who analysed in detail the relative role of slowly varying attractive interactions and rapidly varying repulsive interactions on the frequency shifts and dephasing in liquids. Their theoretical model correctly predicted the isothermal density dependence of the C=CH_2 bandwidth in isobutylene and the C=O bandwidth in acetone.

As a natural extension of our systematic studies of vibrational dephasing, we have become interested in vibrational relaxation in liquids exhibiting strong intermolecular interactions and, therefore ammonia [78] and methanol were investigated.

3.5. Frequency non-coincidence effect

For some strongly polar fluids, the peak frequency of the isotropic Raman line does not coincide with that of the anisotropic line. This frequency difference $\delta\nu$, defined as

$$\delta\nu = \nu_{\text{aniso}} - \nu_{\text{iso}} \tag{26}$$

is called the frequency non-coincidence effect, and it is particularly pronounced for the vibrational bands which are both Raman and infrared active. In early 1970 Mirone and co-workers first studied the non-coincidence effect in carbonyl group containing liquids at ambient conditions. It was found that the $\delta\nu$ can be as large as 30 cm^{-1} for some polar liquids [79]. Theoretical models have been proposed by Wang and McHale [80], McHale [81], Mirone and Fini [82], Mirone [83], Doge *et al* [84], and most recently, by Logan [85,86].

It has been suggested [87,88] that the non-coincidence effect is caused by the transition dipole–dipole coupling in the liquids where short-range order exists due to the strong interactions between permanent dipole moments. However, Wang and McHale [80] have shown that this effect may originate from the angular dependence of the intermolecular potential rather than the short-range order. Based on this idea, McHale [81] has derived an explicit formula of the non-coincidence effect in solution

$$\delta\nu = \frac{8\mu^2\rho}{25(2\pi c)^2 kTd^3\nu m}\left|\frac{\mathrm{d}\mu}{\mathrm{d}Q}\right|^2 \frac{\phi S}{(4\pi\epsilon_0)^2} \tag{27}$$

where d is the distance of closest approach between two molecules of dipole moment μ whose transition dipole moments are coupled, ρ and ϕ is the number density and the volume fraction of the solute, respectively, ν is the vibrational frequency of a free molecule, and S is the dielectric screening factor which is essentially, a function of the dielectric constant of the solution and the index of refraction of the solute.

Logan considered the simple dipolar hard sphere liquid and assumed that the dominant mechanism of non-coincidence effect is the resonant excitonic transfer between the same molecules which are mixed with either isotopic solvents [85] or non-isotopic solvents [86]. Assuming the resonance excitonic transfer is due to the transition dipole-transition dipole coupling, he derived the following equation for $\delta\nu$

$$\delta\nu = X_{\text{A}}\frac{48\xi(\mu,\rho,T)}{25(2\pi c)^2\pi\epsilon_0\nu\sigma^3 m}\left|\frac{\mathrm{d}\mu}{\mathrm{d}Q}\right|^2 \tag{28}$$

where X_{A} is the mole fraction of the probe molecule and a the hard sphere diameter. The local structure factor, $\xi(\mu,\rho,T)$, which can be found by using the mean spherical approximation, is apparently the major difference between this model and that of Wang and McHale [80]. In fact, as proposed by Logan [86], this structure factor, $\xi(\mu,\rho,T)$ not only plays an analogous role to the screening factor, S, in Wang and McHale's model but it also provides a means of elucidating the microscopic, rather than phenomenological, origin of the non-coincidence effect.

To test these two major theoretical models, we investigated the C=O symmetric stretching mode (ν_4) of N,N-dimethylacetamide (DMA) as a function of pressure from 1 to 400 MPa within the temperature range 40 to 100 °C [89]. There were a number of reasons for this choice. As found by Fini and Mirone, the CO stretching mode in several compounds generally has relatively large non-coincidence effect. Although both theoretical models have shown an explicit density dependence of the non-coincidence effect (equations (27) and (28)), most of the experimental studies were done at ambient conditions rather than at different densities (or pressures).

While the pure DMA shows a large non-coincidence effect ($\simeq 10$ cm^{-1}), its solutions, with 5% mole fraction of DMA, diluted by either polar or non-polar solvents do not shown any significant non-coincidence effect (i.e. $\delta\nu < 1$ cm^{-1}). This is expected from the theory that the non-coincidence effect arises from the interactions (i.e. resonant excitonic transfer) between the same (DMA) molecules.

The experimental results of $\delta\nu$ for both acetone [77] and DMA were compared with both theoretical models. It appears that Logan's theory is in closer agreement with the experimental results for both acetone and DMA than is McHale's theory. From the theoretical viewpoint, we would generally expect that $\delta\nu$ is positive and increases as the density is increased isothermally due to the fact that smaller intermolecular distances strengthen the coupling and hence enlarge the splitting. This density dependence has been observed for both acetone and DMA. However, for some other liquids, these predictions are not correct. For example, for both methanol [60] and ethanol [90], $\delta\nu$ is negative and, furthermore, $\delta\nu$ in ethanol decreases as the density is increased isothermally. According to Wang and McHale's theory, if all resonant energy transfer mechanisms are also taken into account, along with the transition-dipole–transition-dipole coupling mechanisms, then $\delta\nu$ can be negative, but still should increase as the density is increased.

Recently, we have investigated the C=O symmetric stretching mode of propylene carbonate (PC), chlorethylene carbonate (CC) and dichloroethylene carbonate (DC) as a function of pressure up to 300 MPa and over the temperature range from 253 K to 313 K [91]. These polar liquids possess different dipole moments and yet, their molecular shapes and sizes are similar. The dipole moment of PC, CC and DC are 4.94, 3.99 and 3.44 Debye, respectively [92]. It was found that Logan theory works very well for pressure dependence when compared with the experimental results of the non-coincidence effect for all three samples. Also, the temperature and density dependence of the non-coincidence effect agree with the theoretical predictions, i.e. $\delta\nu$ increases as density is increased or as temperature is decreased. As an illustration we include figure 12 which shows the density dependence of the $\delta\nu$ for liquid propylene carbonate over the temperature range from 253 to 313 K.

3.6. Collision-induced scattering

The origin of collision induced scattering (CIS) in Rayleigh and Raman spectra lies in the changes of polarizabilities produced by intermolecular interactions; such scattering would be absent without collisions. Therefore, due to the same reasons as mentioned earlier, the high-pressure CIS studies are expected to contribute to the detailed understanding of these phenomena. Since the observation in the depolarized Rayleigh spectra of atomic gases [93], collision-induced scattering has attracted both theoretical and experimental interest. In fact, the CIS effect was suggested as early as 1952 [94]. In their high-pressure Raman scattering experiment of CO_2, Welsh *et al* [94] suggested that the observation of the ν_2 and ν_3 bands, which would not be allowed according

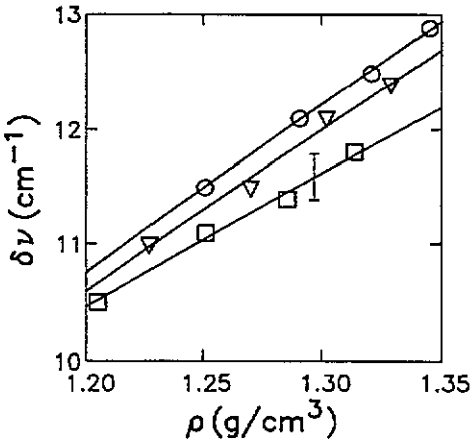

Figure 12. Density dependence of the frequency non-coincidence effect, $\delta\nu$, for liquid propylene carbonate in the temperature range from 253 to 313 K. (Taken from [91].)

to the selection rules of the isolated molecule, is probably due to the distortion of the molecules induced by collisions [95]. Birnbaum collected many excellent review articles about the interaction induced phenomena in light scattering and other fields, such as IR absorption [56]. A rather complete list of references for this problem can be found from the bibliography written by Borysow and Frommhold [96] which covers comprehensively the work of collision-induced light scattering for the last 25 years. Most recently, Frattini *et al* [97] also reviewed the collision-induced effects in Raman and Rayleigh spectra of fluids composed of linear molecules. However, in their article, the emphasis was on the molecular dynamics simulation work. Since this review is not intended to be comprehensive, we will only focus on recent high-pressure work of CIS effects in depolarized Rayleigh scattering (DRS), allowed Raman scattering and forbidden Raman scattering, which will be discussed in this order in the following paragraphs.

Because the depolarized Rayleigh spectrum measures only the correlations between fluctuations in the anisotropic parts of the polarizability, the simplest systems available for the CIS studies are atomic fluids [98] or fluids composed of spherically symmetric molecules such as CH_4 and SF_6 [99]. In these dense fluids, the anisotropic part of the polarizability is entirely collision-induced. However, it is more complicated for the DRS of diatomic [100,101] and linear triatomics [102]. The complication lies in the fact that the time dependence of the polarizability anisotropy of the molecule will contain contributions from both the permanent anisotropy of the molecule, whose time dependence arises from molecular re-orientation, and the induced polarizability which arises from multi-body interactions. The time-scale separation of these two contributions has been proved invalid even in the case of the simplest diatomic molecule such as N_2 [103]. Furthermore, in order to take into account of the re-orientational dependence of the collisional polarizability of a pair of anisotropic molecules, the simplest centre–centre interaction model has to be replaced by the more realistic site–site interaction model. Although, in separating the three contributions from the observed spectrum, the collision-induced part $I^{CI}(\nu)$, has attracted a lot of attention, there are no exact analytical calculations at the present time. Thus, to get a better picture

of CIS effects in dense fluids, in addition to the experiments, the molecular dynamics (MD) simulation turns out to be very helpful. However, there are only a few simple molecular fluids which have MD simulation results, namely N_2, CO_2 [104,100], O_2 [105], and CS_2 [106].

The overall DRS lineshape and the spectral moments, namely the zero moment (i.e. the integrated intensity) and the second moment, are the most commonly used three parameters in the analysis of the CIS effects. In the DRS lineshape of CH_4 at low density, it was shown that the spectra can be separated into two distinct regions [107,108]. The central region (0–150 cm^{-1}) is due to the dipole induced dipole (DID) mechanism, whereas the far region (200–500 cm^{-1}) is due to the collision-induced rotational Raman effect caused by the quadrupole-induced dipole interactions. In our high-pressure studies of both CH_4 and SF_6 liquids [99], we fitted the DID region (25–85 cm^{-1}) of DRS by exponential function of the form of $A\exp(-\nu/\Delta)$ and found that the decay constant Δ for both fluids increase with the density. These results agreed quite well with the theoretical prediction of Ballucani and Vallauri [109]. While there are only two regions in the DRS of fluids composed of optically isotropic molecules, one needs three or even four regions in the fitting of DRS line shape for fluids composed of anisotropic molecules, such as OCS, CS_2 [110,111] and N_2O [112]. As explained earlier, in these linear triatomic molecule systems, we have to consider three contributions to their DRS. The central part of the DRS is dominated by the pure re-orientational motions with some effects due to the cross terms. In contrast, the collision-induced terms contribute to the low frequency as well as to the far wings of DRS line. Due to their slow decay, the cross terms also contribute to the wings [101,113].

However, the density and temperature dependence of these decay constants, Δ, can only provide a qualitative picture of the CIS effects. A quantitative and more detailed understanding of CIS requires MD simulations. A detailed theoretical analysis of depolarized Rayleigh spectra for molecular fluids was given by Ladanyi [101]. Using the DID mechanism between molecular centres (for centre–centre model) or sites (for site–site model) which interacting with each other through a Lennard–Jones potential, Ladanyi decomposed the correlation functions of DRS into three components (i.e. orientational, collision-induced and the crossed terms) and derived explicit expressions for each of them. Since DRS spectrum is simply the Fourier transform of this correlation function, this implies that we can obtain theoretical DRS spectra due to all three processes. Then, by comparing with the experimental results, we can not only determine the relative contributions of these three processes to the DRS, but also find the most appropriate interaction model. The most frequently used experimental results in this comparison are the zero moment (i.e. total DRS intensity), the DRS lineshape, and the second moment, $M(2)$.

The total intensity of the depolarized Rayleigh scattering, I^{tot}, has a very complicated density dependence. To show this density dependence of I^{tot}/ρ, the integrated DRS intensities data of N_2, CO_2, N_2O [114] and O_2 [105] are divided by density and plotted in figure 13. Clearly, for all the studied gases, they show similar trends: I^{tot}/ρ first increases with density, but with a further density increase the intensity decay can be seen. Similar behaviour was also observed by Versmold and Zimmermann [115] in their high-pressure DRS study of ethane. These authors found that the ratio I^{tot}/ρ for ethane decays by a factor of 4 when the density is increased from 160 to 400 amagats. Therefore, on the basis of these experimental results, we have proposed that the density dependence of the ratio I^{tot}/ρ as illustrated in figure 13 is a general observation for linear molecules. Similar behaviour has been observed for atomic gases,

but there is one significant difference between linear molecules and noble gases. For atomic gases, the induced terms are solely responsible for the density dependence of the total intensity, while for linear polyatomic molecules these terms are believed to be small and dominated by the allowed transitions and cross terms.

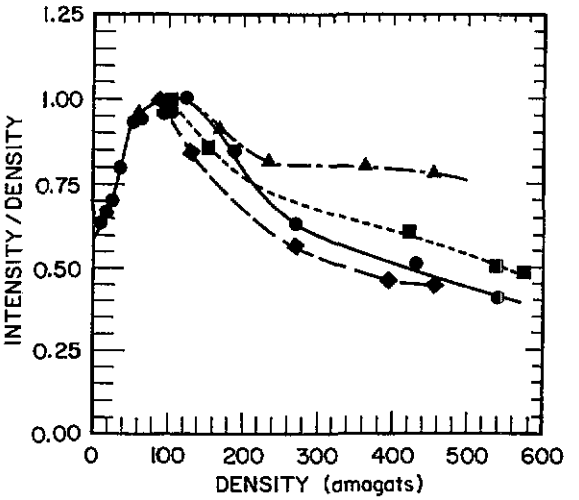

Figure 13. The experimental DRS intensity per one molecule I^{tot}/ρ of N_2 at 298 K (▲); CO_3 at 333 K (■); N_2O at 348 K (♦); and O_2 at 300 K (●). The data are normalized to I^{tot}/ρ at maximum value for each system separately. (Taken from [114].)

Based on the Ladanyi's centre–centre DID perturbation model, the MD simulated DRS spectrum of O_2 was calculated and agrees quite well with the experimental line-shape [105] measured in the pressure range from 2 MPa to 300 MPa and temperature 300 K. It was found that, while the re-orientational contribution dominates the overall band shape, the collision-induced and cross terms become more important at higher density. Furthermore, at lower frequencies, the observed spectrum is smaller than pure re-orientational spectrum which, in turn, indicates the negative contribution of the cross term. In their MD studies of liquid nitrogen, De Santis *et al* [116] also found that the cross term contributed negatively to the DRS. Using DID interaction and the two-body collision model, De Santis *et al* [117] and De Santis and Sampoli [118] analysed the intensity due to the cross term, I^{CR} and found that

$$I^{CR} = \int I^{CR}(\nu)\mathrm{d}\nu = C\left(\frac{16}{75}\right)\rho^2\gamma\left[\alpha^2\tau_{20} + \frac{\gamma^2}{3}\left(\tau_{20} - \frac{\tau_{22}}{5}\right) + \frac{\gamma^2}{9}\left(2\tau_{20} - \frac{\tau_{22}}{5}\right)\right] \quad (29)$$

where τ_{20} and τ_{22} are parameters introduced by Ladanyi and Keyes [119] which, for linear molecules, can be expressed in terms of particular spherical components of the pair distribution function [120]. Since the values of τ_{20} and τ_{22} are generally less than zero, the cross term can be negative and consequently, decrease the total intensity. The total intensity of the depolarized Rayleigh spectrum due to pure re-orientational contribution, I^{OR} is proportional to the number density of the molecule, ρ [116]

$$I^{OR} = \int I^{OR}(\nu)\mathrm{d}\nu = C\tfrac{4}{45}\rho\gamma^2(1 + F_2) \quad (30)$$

where C is a constant, F_2 the orientational pair correlation factor and γ the polarizability anisotropy. Whereas the collision-induced intensity I^{CI}, is given by the approximate formula

$$I^{CR} = \int I^{CR}(\varphi)\mathrm{d}\nu = C\rho\left[\alpha^4(2S_2 + 2S_3 + S_4) + \tfrac{56}{45}\alpha^2\gamma^2(S_2 + S_3) + \tfrac{176}{675}\gamma^4 S_2\right] \quad (31)$$

where S_n are the value of n-body collision-induced correlation functions at time zero. S_2 is positive and proportional to the density ρ, S_3 is negative and proportional to ρ^2 and S_4 is positive and proportional to ρ^3, thus, at the low density limit or in the gas phase where the two-body collisions dominate, the total intensity induced by collisions varies as the square of the density. At higher density or in liquid phase where many-body collisions become important, the collision-induced intensity may vary as the cubic or higher order of density.

The MD spectra of DRS and IR for linear triatomic molecules, such as CO_2 [104,121] and CS_2 [106], were also compared with the corresponding experimental spectra. However, the MD results are strongly dependent on the assumption of the intermolecular interaction, the polarizability model (i.e. centre–centre or site–site) and the origin of the collision-induced scattering. The most commonly used model is the centre–centre model with dipole-induced–dipole mechanism [105]. But at higher densities, intermolecular distances become so small that multipole interaction and electron overlap are also possible. For liquid CO_2, Frattini *et al* [122] compared the difference between two-centre Lennard–Jones potential and three-centre Lennard–Jones potential. Although for molecules the site–site DID model is more realistic (also more complicated) than the centre–centre DID model, Murthy *et al* [123] found that, for the depolarized Rayleigh line of liquid CO_2, S–S and C–C models make no difference at low density and, at high density, the C–C model even works better than the S–S model. In their theoretical study of the orientational order of liquid CO_2, Frattini et al [122] also found that the use of distributed charges instead of a point quadrupole makes no significant difference.

Another evidence of the collision-induced scattering can be found from the density dependence of the second moment. As is well known that classically, the rotational second moment $M(2)$ is related to the rotational kinetic energy and should be density independent. However, we found that $M(2)$ is strongly density dependent in propyne [64] and liquid chloroform [63]. Similar to the total intensity of depolarized Rayleigh peak, the observed second moment $M(2)$ consists of three components: the pure orientational part, $M^{OR}(2)$; the collision-induced part, $M^{CI}(2)$ and the cross term, $M^{CR}(2)$. Many fluids, such as O_2 [105], N_2, CO [100] and CO_2 [104] show similar density dependence of the ratio of the experimental to classical free rotor second moment, $M(2)/M^{OR}(2)$, which reflects the extent of non-orientational effects. For fluid oxygen at 300 K, this ratio first decreases up to about 80 amagats, and a substantial increase is observed at higher densities. Comparing the calculated second moments, $M^{CI}(2)$ and $M^{OR}(2)$ with experimental values, $M(2)$, of the liquid oxygen, it was found that the collision-induced term $M^{CI}(2)$ contributes negatively to the second moment $M(2)$ at low densities and positively at high densities, whereas at lower densities, $M^{CI}(2)$ contributes more negatively to $M(2)$, but $M^{OR}(2)$ contributes less positively to $M(2)$. Since in the low density region, $M^{OR}(2)$ is approximately density-independent, the minimum of the $M(2)/M^{OR}(2)$ curve is determined by the balance of the density dependence of $M^{CI}(2)$ and $M^{CR}(2)$. The minimum of the second moment of DRS versus density was also observed in C_2H_6 [115].

For completely depolarized scattering, the depolarization ratio, $\eta(\nu)$ defined as the ratio of the depolarized intensity $I_{VH}(\nu)$ to the polarized intensity $I_{VV}(\nu)$ is equal to 3/4. However, due to the collision induced scattering $\eta(\nu)$ will be less than 3/4. Based on the dipole-induced dipole model

$$\eta_{DID}(\nu) = \frac{1}{\frac{4}{3} + \frac{I^{CI}(\nu)}{\bar{I}(\nu)}} \tag{32}$$

where $I^{CI}(\nu)$ is the collision-induced scattering intensity. Therefore, investigating $\eta(\nu)$ as a function of density can also disclose the information about the collision-induced interactions. This has been studied for Rayleigh spectra of N_2 [124], CO_2 [125], H_2S [126] and several fluids composed of isotropically polarized molecules [127, 128]. All three systems, O_2, N_2 and CO_2 show similar density dependence of $\eta(\nu)$ with respect to the classical limit, 3/4.

The allowed depolarized Raman scattering arises primarily due to single molecule re-orientation. The theoretical approach for the MD simulation of Raman scattering is similar to that of depolarized Rayleigh scattering [129]. To investigate the CIS effects in allowed Raman scattering, we also measured the depolarized Raman spectra (i.e. O, Q, and S branches centred at 1554.7 cm^{-1}) of fluid oxygen at 300 K over the pressure range of 2–300 MPa and compared with the MD results [130]. The CI and CR interaction-induced contributions to the ratio $M(2)/M^{OR}(2)$ are very similar to that in the depolarized Rayleigh scattering. Both MD and experimental spectra exhibit broadening with increasing density. The experimental line shapes and the density dependence of the experimental second moment agree very well with the MD results. Same as the DRS, the orientational relaxation is dominant over the density range considered and the contribution due to collision-induced terms increases with increasing density. Basically, the same mechanisms are responsible for the second moment of either DRS or Raman spectra, if the rotation–vibration coupling can be neglected. Nevertheless, it was shown that [112] $M^{CI}(2)$ for DRS depends more on the density than that of Raman scattering. In fact, the cross term $M^{CR}(2)$ for O_2 and CO_2 can be even more sensitive to the density than the induced term, $M^{CI}(2)$ [101, 129]. This behaviour was also observed in the study of N_2O [131] at pressures varied from 0.08 MPa to 200 MPa and over temperature range from 298 K to 373 K.

Despite its very weak intensity, studying forbidden bands is the most direct and easiest way for interpretation of the collision-induced interactions. This is due to the fact that there is no symmetry allowed component needed to be separated from the observed spectrum, and the whole band is attributed to multi-body interactions. Two of the most popular and well-studied systems using high-pressure experiments are the linear symmetric molecules CO_2 and CS_2 ([99, 14, 132–134] and references therein) where the bending mode ν_2 and the asymmetric stretching mode ν_3 are infrared-active and Raman forbidden in the isolated molecules. The origin of the collision-induced forbidden bands is explained in terms of two major mechanisms, one involving the dipole–quadrupole polarizability called the $A\alpha$ mechanism, and the other is related to the first hyperpolarizability named the $\beta\theta$ mechanism [135, 136]. For both CO_2 [137, 138] and CS_2 [135, 136], it has been shown that dipole–quadrupole mechanism (i.e. $A\alpha$) dominates [137].

The many-body cancellation effects on the collision-induced intensity at higher densities occur not only for the atomic and spherical-symmetry molecular fluids, but also for the non-spherical molecular fluids such as CO_2. Baglin and his co-workers

investigated the ν_2 forbidden band of carbon dioxide and its solutions with nitrogen at 50 °C and 70 °C over a pressure range from 10 MPa to 300 MPa [139]. One of the interesting results was that the dominant scattering species for the ν_2 band are the pairs of CO_2 (dynamic dimers) rather than individual molecules. These pairs undergo ultrafast intermolecular dynamics processes in time scales ranges from 30 to 60 fs. Furthermore, Yoon *et al* [140] calculated the density dependent integrated intensities of ν_2 based on the quadrupole-induced–dipole (QID) mechanism which agrees quite well with the experimentally determined intensities. In addition, it was shown that the intensities can be expressed as a function of the density squared [140].

If Aα mechanism dominates, then the Raman-forbidden bands should be dependent on the magnitude of the polarizabilities of the neighbouring molecules, but should be less affected by their permanent moments. Therefore, the ν_2 spectrum of CO_2 1 : 1 mixed with the solvent molecules Ar, Xe, N_2, and CO [141] was measured at pressure range from 30 MPa to 240 MPa and at two different temperatures, 313 K and 353 K. There were a number of reasons for choosing these solvents. First, Ar and Xe both have zero permanent moments but very different polarizabilities, $\alpha_{Xe} = 4.02$ and $\alpha_{Ar} = 1.64$. Second, they are completely miscible with CO_2. Third, no other Raman bands are found in the spectral region of interest (450–900 cm^{-1}). The total intensity of CO_2–Ar, $I^{tot}(CO_2\text{–Ar})$, and CO_2–Xe systems, $I^{tot}(CO_2\text{–Xe})$, were found increasing with the density as shown in figure 14, indicating the domination of the two-body collision contributions. Furthermore, the intensity ratio $I^{tot}(CO_2\text{–Xe})/I^{tot}(CO_2\text{–Ar})$ is constant over the densities considered at 313 K and its value is 2.2. Since the multipole moments of the two systems are the same, this density-independent intensity ratio implies that the dipole–quadrupole mechanism may be the dominant contribution to the ν_2 forbidden band of CO_2. Applying the method described by Cox and Madden [135, 136], this intensity ratio due to the Aα mechanism was calculated and its theoretical value of 2.0 was in surprisingly good agreement with the experimental value. The same conclusion may also apply for the CO_2–N_2 and CO_2–CO systems, because their spectral intensities are similar to that of CO_2–Ar system and these solvents have similar polarizabilities [142, 143]. Hence the experimental value of the intensity ratio $I^{tot}(CO_2\text{–CO})/I^{tot}(CO_2\text{–}N_2) = 1.10$ may also be explained by the dominant Aα mechanism ($\alpha_{CO}/\alpha_{N_2} = 1.10$). Ikawa and Whalley [132–134] have investigated CS_2 under pressures up to 1000 MPa at room temperature. They studied the pressure effects on the allowed Raman bands ν_1 and $2\nu_2$ and the forbidden bands ν_2 and ν_3 in terms of the relative intensity, linewidths and peak positions. For the ν_1 mode, they also discussed the pressure effects on the re-orientational and the vibrational correlation times. They observed that the total intensity for ν_2 and ν_3 are approximately linearly proportional to the density which, as suggested by the authors, indicates that these interaction-induced scatterings are caused by the molecular orientational fluctuations rather than the translational fluctuations.

In addition to the references mentioned above, other important high-pressure Rayleigh and Raman scattering studies have also been carried out since 1985. Some of these experimental studies are summarized in tables 4 and 5 for the Raman and Rayleigh scattering, respectively.

Acknowledgments

This work was supported in part by the National Science Foundation under grant NSF CHE 90-17649 and the Air Force Office for Scientific Research under grant AFOSR

Table 4. Recent Raman studies of fluids at high pressure.

Liquid	Experimental range		Property studied[a]	Ref.
	T (K)	P (MPa)		
Oxygen O_2	300	4–300	MT, CF	[130]
Hydrogen H_2 and	123	0.1–2.6	DR	[144]
mixtures with	100–300	0.1–50	LW	[145]
Ne, Ar, Kr				
Nitrogen N_2	79–125.7	0.1–250	LW, FS	[146]
Carbon disulfide	293–353	0.1–300	FS	[91]
CS_2	295	0.1–1000	LW, FB, CIS	[132], [134], [133]
	273, 298	35–245	CF	[14]
Carbon dioxide and	323	0.1–216	FR	[147]
its solutions with	323, 343	1–300	CIS, FB	[140]
N_2 and Ar, Xe	323	0.1–285	CIS, FB, DR	[148]
	323, 348	9–301	MT, CIS, FB	[139]
	313, 353	8–180	DR, CIS, FB	[141]
Nitrogen N_2, Carbon monoxide CO and their mixtures in He Ar, Kr	277–300	0.1–1.5	LW	[149]
Nitrous oxide N_20	298–423	0.8–200	LW, NE	[150]
	298–373	0.8 - 200	MT, CF	[151]
Ammonia: NHD_2,NH_3	273–373	0.1 - 200	LW, FR	[69], [152]
Methylhalides:	323	2.8–160	CF, LW	[153]
CH_3F; CH_3I, CD_3I	293	0.1–400	FS, LW	[154]
Methane CH_4	293	0.1–300	FS, LW	[155]
Carbon tetrachloride	295	0.1–110	DR	[156]
Methanol and	273–363	1–400	FS, LW, FR, NE	[60], [157]
its mixtures	273–371	0.1–300	NE	[90]
with Ethanol	room	0.1–6000	FS, LW	[158]
Ethanol	273–371	0.1–300	NE	[90]
	300	0.1–17000	FS	[159]
Water	443, 473	0.1–36000	FS	[160]
	300–800	0.1–1.6	LW, CARS	[161]
Ethane C_2H_6	323	0.1–200	CIS, MT, CF	[115]
Pyridine in aqueous solution	298	0.1–3500	FS, FR	[162]
Benzene	298–448	0.1–1200	FS	[163]
Toluene	293, 373	0.1–400	FS	[164], [61], [67]
Nitromethane: CH_3NO_2, CD_3NO_2, CH_3, $^{15}NO_2$	298, 373	0.1–2000	FS	[165]
N, N-dimethylacetamide	313–373	0.1–400	LW, NE	[89]
Propylene carbonate, Chloroethylene carbonate, and Dichloroethylene carbonate	253–313	0.1–300	NE	[91]

[a] CIS: collision induced scattering; FS: frequency shift; LW: linewidth; MT: spectral moment; CF: correlation functions; FB: forbidden band, FR: fermi resonance; NE: non-coincidence effect; DR: depolarization ratio; CARS: coherent anti-stokes Raman scattering.

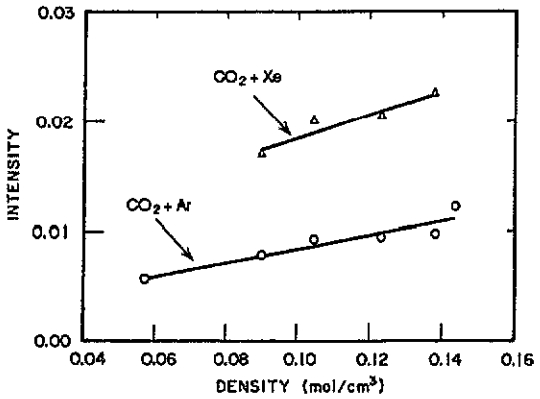

Figure 14. Relative intensities of the forbidden ν_2 band of CO_2 in Ar (O) and Xe (Δ) mixtures plotted as a function of density at 313 K. (Taken from [141].)

Table 5. Recent Rayleigh scattering studies of fluids at high pressure.

Liquid	Experimental range		Property studied[a]	Ref.
	T (K)	P (MPa)		
Oxygen O_2	300	1–300	MT, CF	[105]
Hydrogen H_2	123	0.1–2.6	DR	[144]
	297	4–10	CIS, MT	[166]
Nitrogen N_2	298	0.1–300	CIS	[114]
Carbon disulfide CS_2	293–353	0.1–300	MT, CF	[111]
Carbon dioxide	313	20–270	MT, CF	[167]
CO_2	333	0.1–300	CIS	[114]
Nitrous oxide	298–373	0.1–200	MT, CF	[151]
N_20	348	0.1–300	CIS	[114]
Methane CH_4 and its mixtures with Ar, Xe	297	0.1–20	CIS	[168]
Ethane C_2H_6	323–398	0.1–200	MT, CF	[67]
	323		MT, CF	[115]

[a] Same notation as in table 4.

89-0099. We express our thanks to Professor H-D Lüdemann for his permission of reproducing figure 4 and to Professor D R Herschbach for his permission of reproducing figure 9.

References

[1] Jonas J 1984 *Acc. Chem. Res.* **17** 74
[2] Jonas J and Lamb D M 1987 *ACS Symp. Ser.* **329** 17
[3] Drickamer H G 1987 *NATO ASI Ser. C* **197** 263
[4] Schindler W, Zerda T W and Jonas J 1984 *J. Chem. Phys.* **81** 4306
[5] Peng X and Jonas J 1990 *J. Chem. Phys.* **93** 2192

[6] Jonas J 1987 *NATO ASI Ser. C* **197** 196
[7] Bradley M, Zerda T W and Jonas J 1984 *Spectrochim. Acta* A **40** 1117
[8] Lang E W and Lüdemann H D 1991 *NMR Basic Principles and Progress* vol 24 (Berlin: Springer) p 129
[9] Franck E U 1987 *Pure Appl. Chem.* **59** 25
[10] Hensel F 1987 *NATO ASI Ser. C* **197** 117
[11] Wakeham W A 1989 *High Temp. – High Pressures* **21** 249
[12] Schneider G M, Ellert J, Haasbus V, Holscher J F, Katzenski-Ohling G, Kopner A, Kulka J, Nickel D, Rubesam J and Wilsch A 1987 *Pure Appl. Chem.* **59** 1115
[13] Ross M 1987 *NATO ASI Ser. C* **197** 9
[14] Baglin F G 1987 *Spectroscopy* **2** 26
[15] Jonas J 1982 *Science* **216** 1179
[16] Walker N, Lamb D M, Jonas J and Dare-Edwards M P 1987 *J. Magn. Resonance* **74** 580
[17] Lamb D M, Grandinetti P J and Jonas J 1987 *J. Magn. Resonance* **72** 532
[18] Jonas J 1980 *Rev. Phys. Chem. Japan* **50** 19
[19] Jonas J 1975 *Ann. Rev. Phys. Chem.* **26** 167
[20] Chandler D 1975 *J. Chem. Phys.* **62** 1358
[21] Alder B J, Gass D M and Wainwright T E 1970 *J. Chem. Phys.* **53** 3813
[22] Dymond J H 1974 *J. Chem. Phys.* **60** 969
[23] Fury M, Munie G Munie and Jonas J 1979 *J. Chem. Phys.* **70** 1260
[24] Jonas J, Hasha D and Huang S G 1979 *J. Chem. Phys.* **71** 3996
[25] Speedy R J, Prielmeier F X, Vardag T, Lang E Wand Lüdemann H D 1989 *Mol. Phys.* **66** 577
[26] Lüdemann H D 1990 *Ber. Bunsenges. Phys. Chem.* **94** 325
[27] Hurle R L, Easteal A J and Woolf L A 1985 *J. Chem. Soc. Faraday Trans.* **1 81** 769
[28] Easteal A J and Woolf L A1984 *J. Chem. Soc. Faraday Trans.* **1** 80 549
[29] Easteal A J and Woolf L A 1985 *J. Chem. Soc. Faraday Trans.* **1 81** 2821
[30] Prielmeier F X, Lang E W and Lüdemann H D 1984 *Mol. Phys.* **52** 1105
[31] Has M 1989 *Diplomarbeit* Universität Regensburg
[32] Prielmeier F X and Lüdemann H D 1986 *Mol. Phys.* **58** 593
[33] Harris K R, Lam H N and Raedt E 1990 *Mol. Phys.* **71** 1205
[34] Vardag T M and Lüdemann H D 1988 *Chem. Phys.* **128** 527
[35] Harris K R 1978 *Physica* A **93** 593
[36] Walker N A, Lamb D M, Adamy S T and Jonas J 1988 *J. Phys. Chem.* **92** 3675
[37] Jonas J, Adamy S T, Grandinetti P J, Masuda Y,Morris S J, Campbell D M and Li Y 1990 *J. Phys. Chem.* **94** 1157 .
[38] Lang E W, Prielmeier F X, Radkowitsch H and Lüdemann H D 1987 *Ber. Bunsenges. Phys. Chem.* **91** 1017
[39] Lamb W J, Brown D R and Jonas J 1981 *J. Phys. Chem.* **85** 3883
[40] Tyrell H S K and Harris K R 1984 *Diffusion in Liquids* (London: Butterworths) p 259
[41] Jonas J, Hasha D and Huang S G 1980 *J. Phys. Chem.* **84** 109
[42] Parkhurst H G and Jonas J 1975 *J. Chem. Phys.* **63** 2698
[43] Gierer A and Wirtz K 1953 *Z. Naturforsch.* A**8** 532
[44] Jonas J 1990 *Ber. Bunsenges. Phys. Chem.* **94** 307
[45] Akitt J W and Mehrbach A E 1991 *NMR, Basic Principles and Progress* vol 24 (Berlin: Springer) p 189
[46] Jonas J 1991 *NMR, Basic Principles and Progress* vol 24 (Berlin: Springer) p 85
[47] Yamada H 1991 *NMR, Basic Principles and Progress* vol 24 (Berlin: Springer) p 233
[48] Jonas J, Xie C-L, Jonas A, Grandinetti P J, Campbell D M and Driscoll D 1988 *Proc. Natl Acad. Sci. USA* **85** 4115
[49] Adamy S T, Grandinetti P J, Masuda Y, Campbell D M and Jonas J 1991 *J. Chem. Phys.* **94** 3568
[50] Wolfe M and Jonas J 1979 *J. Chem. Phys.* **71** 3252
[51] Wilbur D J and Jonas J 1973 *J. Magn. Resonance* **10** 279
[52] Linowski J W, Liu Nan-I and Jonas J 1976 *J. Magn. Resonance* **23** 455
[53] Linowski J W, Liu Nan-I and Jonas J 1977 *J. Chem. Phys.* **66** 760
[54] Schulman E M, Dwyer D W and Doetschman D C 1990 *J. Phys. Chem.* **94** 7308
[55] Jonas J and Akai J A 1977 *J. Chem. Phys.* **66** 4946
[56] Birnbaum G (ed) 1983 *Phenomena Induced by Molecular Interactions (NATO ASI Series B)*

vol 127 (New York: Plenum)
[57] Benson A M Jr and Drickamer H G 1957 *J. Chem. Phys.* **27** 1164
[58] Schweizer K S and Chandler D 1982 *J. Chem. Phys.* **76** 2296
[59] Pratt L R, Hsu C S and Chandler D 1978 *J. Chem. Phys.* **68** 4202
[60] Zerda T W, Thomas H D, Bradley M and Jonas J 1987 *J. Chem. Phys.* **86** 3219
[61] Zakin M and Herschbach D R 1986 *J. Chem. Phys.* **85** 2376
[62] Zakin M and Herschbach D R 1988 *J. Chem. Phys.* **89** 2380
[63] (a) Schroeder J, Schiemann V H and Jonas J 1977 *J. Mol. Phys.* **34** 1501
(b) 1978 *J. Chem. Phys.* **69** 5479
[64] Zerda T W, Perry S and Jonas J 1981 *Chem. Phys. Lett.* **83** 600
[65] Alder B J, Weiss J J and Strauss M L 1973 *Phys. Rev.* **47** 281
[66] Alder B J, Strauss M L and Weiss J J 1973 *J. Chem. Phys.* **59** 1002
[67] Baglin F G, Versmold H and Zimmermann U 1984 *Mol. Phys.* **53** 1225
[68] Oxtoby D W 1981 *Ann. Rev. Phys. Chem.* **32** 77
[69] Fischer S F and Laubereau A 1975 *Chem. Phys. Lett.* **35** 6
[70] Oxtoby D W and Rice S A 1979 *Chem. Phys. Lett.* **42** 1
[71] Oxtoby D W 1979 *J. Chem. Phys.* **70** 2605
[72] Diestler D J and Manz J 1977 *Mol. Phys.* **33** 227
[73] Madden P A 1982 *Raman Spectroscopy—Linear and Non-linear* ed J Lascombe and P V Huong (New York: Wiley)
[74] (a) Schindler W and Jonas J 1980 *J. Chem. Phys.* **72** 5019
(b) 1980 *J. Chem. Phys.* **73** 3547
[75] Rothschild W G 1976 *J. Chem. Phys.* **65** 455
[76] Kubo R 1962 *Fluctuations, Relaxation, and Resonance in Magnetic Systems* ed D Ter Haar (New York: Plenum)
[77] (a) Bull T E and Jonas J 1970 *J. Chem. Phys.* **52** 2779
(b) Schindler W and Jonas J 1979 *J. Chem. Phys. Lett.* **67** 428
(c) Schindler W, Sharko P T and Jonas J 1982 *J. Chem. Phys.* **76** 3493
[78] Bradely M, Zerda T W and Jonas J 1985 *J. Chem. Phys.* **82** 4007
[79] Fini G and Mirone P 1983 *J. Chem. Phys.* **79** 639
[80] Wang C H and McHale J 1980 *J. Chem. Phys.* **72** 4039
[81] McHale J 1982 *J. Chem. Phys.* **77** 2705
[82] Mirone P and Fini G 1979 *J. Chem. Phys.* **71** 2241
[83] Mirone P 1982 *J. Chem. Phys.* **77** 2074
[84] Doge G, Khuen A and Yarwood J 1984 *Mol. Phys.* **52** 399
[85] Logan D E 1986 *Chem. Phys.* **103** 215
[86] Logan D E 1989 *Chem. Phys.* **131** 199
[87] Fini G, Mirone P and Fortunato B 1973 *J. Chem. Soc. Faraday Trans.* II **69** 1243
[88] Fini G Fini and Mirone P Mirone 1974 *J. Chem. Soc. Faraday Trans.* II **70** 1776
[89] Thomas H D and Jonas J 1989 *J. Chem. Phys.* **90** 4144
[90] Thomas H D and Jonas J 1989 *J. Chem. Phys.* **90** 4632
[91] Sun T F, Chan J B, Wallen S L and Jonas J 1991 *J. Chem. Phys.* **94** 7486
[92] McClellan A L 1974 *Table of Experimental Dipole Moments* vol 2 (EL Cerrito CA: Rahara Enterprises)
[93] McTague J P and Birnbaum G 1968 *Phys. Rev. Lett* **21** 661
[94] Welsh H L, Pashler P E and Stoicheff B P 1952 *Can. J. Phys.* **30** 99
[95] Steele W A and Posch H A 1985 *Phenomena Induced by Intermolecular Interactions* ed G Birnbaum (New York: Plenum) p 549
[96] Borysow A and Frommhold L 1989 *Adv. Chem. Phys.* **75** 439
[97] Frattini R, Sampoli M and Vallauri R 1989 *J. Mol. Liquids* **43** 293
[98] Bratos S, Guillot B and Birnbaum G 1985 *Phenomena Induced by Intermolecular Interactions* ed G Birnbaum (New York: Plenum) p 363
[99] Jonas J 1985 *Phenomena Induced by Intermolecular Interactions* ed G Birnbaum (New York: Plenum) p 525
[100] Santis A De and Sampoli M 1985 *Phenomena Induced by Intermolecular Interactions* ed G Birnbaum (New York: Plenum) p 627
[101] Ladanyi B 1983 *J. Chem. Phys.* **78** 2189
[102] Madden P A 1985 *Phenomena induced by intermolecular interactions* ed G Birnbaum (New

York: Plenum) p 399, 643
[103] Frenkel D and McTague J P 1980 *J. Chem. Phys.* **72** 2801
[104] Santis A De and Sampoli M 1984 *Mol. Phys.* **53** 717
[105] Zerda T W, Song X, Jonas J, Ladanyi B M and Geiger L C 1987 *J. Chem. Phys.* **87** 840
[106] Geiger L C and Ladanyi B M 1988 *J. Chem. Phys.* **89** 6589
[107] Buckingham A D and Tabisz G C 1978 *Mol. Phys.* **36** 583
[108] Shelton D P and Tabisz G C 1980 *Mol. Phys.* **40** 285
[109] Ballucani V and Vallauri R 1979 *Mol. Phys.* **38** 1099
[110] Hegemann B and Jonas J 1983 *J. Chem. Phys.* **79** 4683
[111] Hegemann B and Jonas J 1985 *J. Chem. Phys.* **82** 2845
[112] Zerda T W, Song X and Jonas J 1986 *J. Phys. Chem.* **90** 771
[113] De Santis A and Sampoli M 1984 *Mol. Phys.* **51** 1
[114] Song X, Jonas J and Zerda T W 1989 *J. Phys. Chem.* **93** 6887
[115] Versmold H and Zimmermann U 1987 *J. Chem. Soc. Faraday Trans.* 2 **83** 1815
[116] De Santis A, Sampoli M and Vallauri R 1984 *Mol. Phys.* **53** 695
[117] De Santis A, Moretti E and Sampoli M 1982 *Mol. Phys.* **46** 1271
[118] De Santis A and Sampoli M 1984 *Mol. Phys.* **51** 91
[119] Ladanyi B M and Keyes T 1977 *Mol. Phys.* **33** 1063
[120] Frattini R, Gazzillo D, Sampoli M and Vallauri R 1989 *Mol. Simulation* **3** 337
[121] Steele W A and Posch H A1987 *J. Chem. Soc. Faraday Trans.* II **83** 1843
[122] Frattini R, Gazzillo D, Sampoli M and Vallauri R 1989 *Chem. Phys.* **138** 337
[123] Murthy C S, Singer K, R. Vallauri, Versmold H and Zimmermann U 1985 *Berich. Buns. Phys. Chem.* **89** 18
[124] Barreau A, Berrue J, Chave A, Dumon B and Thibeau M 1985 *Opt. Commum.* **55** 99
[125] Santis A De and Sampoli M 1983 *Chem. Phys. Lett.* **96** 114
[126] Santis A De and Sampoli M 1983 *Chem. Phys. Lett.* **102** 425
[127] Posch H A 1982 *Mol. Phys.* **46** 1213
[128] Tabisz G C, Meinander and Penner A R 1985 *Phenomena Induced by Intermolecular Interactions* ed G Birnbaum (New York: Plenum) p 345
[129] Ladanyi B M and Levinger N E 1984 *J. Chem. Phys.* **81** 2620
[130] Ladanyi B M, Geiger L C, Zerda T W, Song X and Jonas J 1988 *J. Chem. Phys.* **89** 660
[131] Zerda T W, Song X and Jonas J 1985 *Chem. Phys.* **94** 427
[132] Ikawa S and Whalley E 1986 *J. Phys. Chem.* **85** 2538
[133] Ikawa S and Whalley E 1987 *J. Phys. Chem.* **86** 1836
[134] Ikawa S and Whalley E 1990 *J. Phys. Chem.* **94** 7834
[135] Cox T I and Madden P A 1980 *Mol. Phys.* **39** 1487
[136] Cox T I and Madden P A 1981 *Mol. Phys.* **43** 287 & 307
[137] Holzer W and Ouillon R 1978 *Mol. Phys.* **36** 817
[138] Madden P A and Cox T I 1985 *Mol. Phys.* **56** 223
[139] Hacura A, Yoon J and Baglin F G, 1989 *J. Chem. Phys.* **91** 5218
[140] Yoon J, Hacura A and Baglin F G 1989 *J. Chem. Phys.* **91** 5230
[141] Song X, Frattini R and Jonas J 1988 *J. Chem. Phys.* **89** 156
[142] Bridge N J and Buckingham A D 1966 *Proc. R. Soc.* A **295** 334
[143] Gray C G and Gubbins K E 1984 *Theory of Molecular Fluids* vol 1 (Oxford: Clarendon)
[144] Le Duff Y and Ouillon R 1985 *J. Chem. Phys.* **82** 1
[145] Robert D, Bonamy J, Sala J P, Levi G and Marsault-Herail F 1985 *Chem. Phys.* **99** 303
[146] Oksengorn B, Fabre D, Lavorel B, Saint-Loup R and Berger H 1991 *J. Chem. Phys.* **94** 1774
[147] Hacura A, Brodka A, Nikiel L and Baglin F G 1990 *J. Mol. Structure* **218** 297
[148] Hacura, A Yoon. J H and Baglin F G 1987 *J. Raman Spectrosc.* **18** 377
[149] Golubev N S, Orlov N D and Khamitov R 1987 *Opt. Spectrosc.* **62** 594
[150] Zerda T W, Song X and Jonas J 1985 *Chem. Phys.* **94** 427
[151] Zerda T W, Song X and Jonas J 1986 *J. Phys. Chem.* **90** 771
[152] Stryczek B and Brodka A 1987-*Mol. Phys.* **62** 365
[153] Gompft J and Versmold H 1984 *Ber. Bunsenges. Phys. Chem.* **88** 733
[154] Doge G and Lindner D 1990 *Ber. Bunsenges. Phys Chem.* **94** 408
[155] Fabre D and Couty R 1986 *C. R. Acad. Sci., Paris* 303 Serie II 1305
[156] Ikawa S and Whalley E 1988 *J. Chem. Phys.* **89** 51
[157] Zerda T W, Bradley M and Jonas J 1985 *Chem. Phys. Lett.* **117** 566

[158] Lemos V and Camargo F 1990 *J. Raman Spectrosc.* **21** 123
[159] Shimizu H, Nakamichi Y and Sasaki S 1990 *J. Raman Spectrosc.* **21** 703
[160] Walrafen G E, Hokmabadi M S, Yang W H and Piermarini G J 1988 *J. Phys. Chem.* **92** 4540
[161] Greenhalgh D A, Hall R J, Porter F M and England W A 1984 *J. Raman Spectrosc.* **15** 71
[162] Zakin M R, Grubb S G, King H E Jr and Herschbach D R 1986 *J. Chem. Phys.* **84** 1080
[163] Zakin M R and Herschbach D R 1985 *J. Chem. Phys.* **83** 6540
[164] Gardiner D J, Walker N A and Dare-Edwards M P 1987 *Spectrochim. Acta* A **43** 1241
[165] Miller P J, Block S and Piermarini G J 1989 *J. Phys. Chem.* **93** 462
[166] Bafile U, Ulivi L and Zoppi M 1988 *Phys. Rev.* A **37** 4133
[167] Geiger L C, Ladanyi B M and Chapin N E 1990 *J. Chem. Phys.* **93** 4533
[168] Penner A R, Meinander N and Tabisz G C 1985 *Mol. Phys.* **54** 479